Journal of Computational Physics 432 (2021) 110159

Contents lists available at ScienceDirect

Journal of Computational Physics

www.elsevier.com/locate/jcp

Conservative semi-Lagrangian schemes for kinetic equations Part I: Reconstruction

Seung Yeon Cho [a,*], Sebastiano Boscarino [a], Giovanni Russo [a], Seok-Bae Yun [b]

[a] Department of Mathematics and Computer Science, University of Catania, Catania 95125, Italy
[b] Department of Mathematics, Sungkyunkwan University, Suwon 440-746, Republic of Korea

ARTICLE INFO

Article history:
Available online 28 January 2021

Keywords:
Conservative reconstruction
Semi-Lagrangian method
Relaxation limit
Broadwell model
Xin-Jin model

ABSTRACT

In this paper, we propose and analyze a reconstruction technique which enables one to design high-order conservative semi-Lagrangian schemes for kinetic equations. The proposed reconstruction can be obtained by taking the sliding average of a given polynomial reconstruction of the numerical solution. A compact representation of the high order conservative reconstruction in one and two space dimension is provided, and its mathematical properties are analyzed. To demonstrate the performance of proposed technique, we consider implicit semi-Lagrangian schemes for kinetic-like equations such as the Xin-Jin model and the Broadwell model, and then solve related shock problems which arise in the relaxation limit. Applications to BGK and Vlasov-Poisson equations will be presented in the second part of the paper.

1. Introduction

Kinetic equations and quasi-linear systems of conservation laws are strongly related. For example, the behavior of rarefied gas is well described by the Boltzmann transport equation (BTE) [1]. Once velocity space is discretized, BTE has the mathematical structure of a semi-linear hyperbolic system of balance laws. In the so-called fluid dynamic limit, the distribution function approaches the Maxwellian whose parameters satisfy the Euler equations of gas dynamics, which is a quasi-linear system of conservation laws. The Broadwell model of the BTE in one space dimension is a semi-linear 3×3 relaxation system. As the relaxation parameter vanishes, the model relaxes to a 2×2 quasi-linear hyperbolic system of conservation laws. An implicit treatment of the collision term using L-stable schemes allows the construction of asymptotic preserving schemes which become consistent schemes of the relaxed limit [2–4].

Quasi-linear hyperbolic systems generically develop jump discontinuities in finite time. Most schemes for their numerical solutions are based on two fundamental ingredients: conservation and non-oscillatory reconstruction. Finite volume and finite difference methods have been widely used for the discretization of the convective terms of kinetic models (Eulerian approach), which are usually treated explicitly. In this way, it is relatively easy to construct conservative schemes. Conservation is relevant especially in the relaxed limit: lack of conservation will prevent weak consistency of the method for discontinuous solutions leading, for example, to $\mathcal{O}(1)$ errors in the propagation of shocks.

Conservative non-oscillatory reconstruction such as the essentially non-oscillatory (ENO) or weighted essentially non-oscillatory (WENO) methodology [5] have been widely adopted in many practical problems [6–8]. The approach has been

* Corresponding author.
E-mail addresses: chosy89@skku.edu (S.Y. Cho), boscarino@dmi.unict.it (S. Boscarino), giovanni.russo1@unict.it (G. Russo), sbyun01@skku.edu (S.-B. Yun).

https://doi.org/10.1016/j.jcp.2021.110159
0021-9991/

extended to a compact WENO (CWENO [9–14]) reconstruction which gives uniform accuracy in a whole cell, and it allows the construction of efficient high order finite volume scheme in several space dimensions [15]. Unfortunately, explicit Eulerian schemes cannot avoid CFL-type time step restrictions imposed by convection-like terms in hyperbolic equations.

To treat this difficulty, semi-Lagrangian approaches recently have gained popularity because they do not suffer from such CFL-type time step restriction which arises in the treatment of Eulerian counterparts. Instead, since the semi-Lagrangian method is obtained by integrating the equations along its characteristics, this approach necessarily requires the computation of numerical solutions on off-grid points by a reconstruction which makes use of the numerical solutions on grid points.

If one uses piecewise Lagrange polynomial reconstruction, then conservation is guaranteed if the same stencil is used in each cell, because of translation invariance (we shall call this a *linear reconstruction*). On the other hand, such linear reconstruction may introduce spurious oscillations or may cause loss of positivity. If one wants to prevent appearing of spurious oscillations, then one can use high-order non-oscillatory reconstruction, such as ENO or WENO [5,6,16]. Similarly, positivity of the numerical solution can be maintained by positivity-preserving reconstructions [17,18]. Unfortunately these non-linear reconstructions destroy the translation invariance guaranteed by linear reconstruction, causing lack of conservation [19].

Numerous approaches have been introduced to treat such difficulties, and maintain conservation even with non-linear reconstruction. In particular, in the context of Vlasov-Poisson system several techniques were proposed. Among them, we mention the Flux-form semi-Lagrangian (FFSL) schemes based on primitive polynomial reconstruction [20–23]. In [20], the authors developed the Positive and Flux Conservative scheme. The authors considered essentially non-oscillatory method (ENO) or reconstructions based on positive limiters. In [21], the authors took a similar approach in the construction of primitive functions using splines. A WENO approach is also proposed to construct high order conservative non-oscillatory schemes in [22,23]. All these methods are either one-dimensional or they provide a dimension by dimension interpolation. A general technique to restore conservation in semi-Lagrangian schemes was presented in [24]. The technique has been also applied to the BGK model [19]. Although quite general, the technique suffers from CFL-type stability restrictions.

In this paper we present a general scheme which is somehow related to FFSL scheme and allows the construction of high-order conservative non-oscillatory semi-Lagrangian schemes in one and several dimensions, which are not affected by CFL-type restriction. In the context of finite volume schemes, given cell averaged values of the solutions on uniform grids, the idea is to compute sliding average of a precomputed non-oscillatory piecewise polynomial reconstruction (from cell averages to point-wise values), thus obtaining a conservative mapping from cell averages to cell averages. In this paper we call the piecewise polynomial reconstruction *'basic reconstruction'*. We remark that the same technique can be adopted in the context of finite difference schemes to provide a conservative mapping from point-wise values to point-wise values.

The resulting reconstruction inherits the non-oscillatory properties of the precomputed polynomial and guarantees conservation of all discrete moments. The technique requires characteristic lines are parallel, which is the case of kinetic equations in which velocity space is discretized on the same velocity grid throughout space. An advantage of our method is that one can easily adopt previous techniques such as ENO, WENO, CWENO polynomials as our basic reconstructions.

The mathematical properties of the proposed reconstruction are analyzed. In particular, we show that if we take CWENO polynomials of even degree k, for example $k = 2, 4$ [9,13], as a basic reconstruction, our approach gives $k + 2$th order accuracy. Similar properties are also generalized to two dimensional reconstruction with CWENO polynomial in two space dimensions [13].

To test the quality of the proposed reconstruction, we apply it to the finite difference implicit semi-Lagrangian schemes for semi-linear hyperbolic system such as Xin-Jin model or Broadwell model. Applications to more general equations will be presented in a companion paper.

This paper is organized as follows: In section 2, we present a general framework for our conservative reconstruction in 1D and its related properties, section 3 is devoted to the conservative reconstruction in 2D. Semi-Lagrangian methods are described in section 4. In section 5, several numerical tests are presented to verify the accuracy of the proposed schemes and its capability in treating shocks arising in the relaxation of semi-linear hyperbolic system.

2. Conservative reconstruction in 1D

Let $u : \mathbb{R} \to \mathbb{R}$ be a smooth function and $\bar{u} : \mathbb{R} \to \mathbb{R}$ be a corresponding sliding average function:

$$\frac{1}{\Delta x} \int_{x-\Delta x/2}^{x+\Delta x/2} u(y)\, dy = \bar{u}(x).$$

Given cell averages on uniform grids $x_i = i\Delta x$:

$$\frac{1}{\Delta x} \int_{I_i} u(x)\, dx = \bar{u}_i, \quad I_i = [x_{i-\frac{1}{2}}, x_{i+\frac{1}{2}}],$$

for each $i \in \mathcal{I}$, our goal is to construct an approximation $Q(x)$ of the sliding average $\bar{u}(x)$, which is conservative in the sense that for any periodic function $\bar{u}(x)$ with period $L = N\Delta x$, $N \in \mathbb{N}$, we have

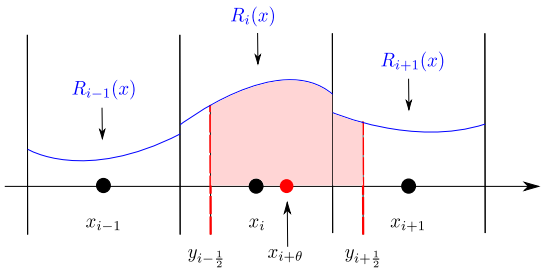

Fig. 1. Description of one-dimensional conservative reconstruction.

$$\sum_{i=1}^{N} Q\left(x_i+\theta\right)=\sum_{i=1}^{N} \bar{u}(x_i), \quad \theta \in [0,1).$$

Assume we have a piecewise smooth reconstruction $R(x)=\sum_i R_i(x)\chi_i(x)$, for $i \in \mathcal{I}$, where $\chi_i(x)$ denotes the characteristic function of cell i and each $R_i(x)$ denotes a polynomial of degree k and has the following properties:

1. High order accuracy in the approximation of $u(x)$:

$$u(x)=R_i(x)+\mathcal{O}\left((\Delta x)^{k+1}\right), \quad x \in I_i. \tag{1}$$

2. Conservation in the sense of cell averages:

$$\frac{1}{\Delta x}\int_{x_{i-\frac{1}{2}}}^{x_{i+\frac{1}{2}}} R_i(x)\,dx=\bar{u}_i.$$

Consider a shifted interval $[y_{i-\frac{1}{2}}, y_{i+\frac{1}{2}}]$ whose center is $x_{i+\theta}\equiv x_i+\theta\Delta x$, $\theta\in[0,1)$, and denote by $\bar{u}(x_{i+\theta})$ the sliding average of u at $x_{i+\theta}$ (see Fig. 1). We see that

$$x_{i-\frac{1}{2}} \le y_{i-\frac{1}{2}} < x_{i+\frac{1}{2}} \le y_{i+\frac{1}{2}} < x_{i+\frac{3}{2}}.$$

Our strategy is to approximate $\bar{u}(x_{i+\theta})$ by $Q_{i+\theta}\equiv Q\left(x_{i+\theta}\right)$, where

$$Q_{i+\theta}=\frac{1}{\Delta x}\int_{y_{i-\frac{1}{2}}}^{y_{i+\frac{1}{2}}} R(x)\,dx=\frac{1}{\Delta x}\int_{x_{i-\frac{1}{2}+\theta}}^{x_{i+\frac{1}{2}+\theta}} R(x)\,dx, \tag{2}$$

which is equivalent to

$$Q_{i+\theta}=\frac{1}{\Delta x}\int_{x_{i-\frac{1}{2}+\theta}}^{x_{i+\frac{1}{2}}} R_i(x)\,dx+\frac{1}{\Delta x}\int_{x_{i+\frac{1}{2}}}^{x_{i+\frac{1}{2}+\theta}} R_{i+1}(x)\,dx. \tag{3}$$

From now on, we consider $R_i(x)$ to be piecewise polynomials of degree k of the form:

$$R_i(x)=\sum_{\ell=0}^{k}\frac{R_i^{(\ell)}}{\ell!}(x-x_i)^{\ell}. \tag{4}$$

Making use of (4) in the first term, we obtain

$$\frac{1}{\Delta x}\int_{x_{i-\frac{1}{2}+\theta}}^{x_{i+\frac{1}{2}}} R_i(x)\,dx=\frac{1}{\Delta x}\sum_{\ell=0}^{k} R_i^{(\ell)}\int_{x_{i-\frac{1}{2}+\theta}}^{x_{i+\frac{1}{2}}}\frac{1}{\ell!}(x-x_i)^{\ell}\,dx=\sum_{\ell=0}^{k}(\Delta x)^{\ell}R_i^{(\ell)}\alpha_{\ell}(\theta)$$

where

$$\alpha_\ell(\theta) = \frac{1-(2\theta-1)^{\ell+1}}{2^{\ell+1}(\ell+1)!}. \tag{5}$$

Similarly, we can write

$$\frac{1}{\Delta x}\int_{x_{i+\frac{1}{2}}}^{x_{i+\frac{1}{2}+\theta}} R_{i+1}(x)\,dx := \sum_{\ell=0}^{k}(\Delta x)^\ell R_{i+1}^{(\ell)}\beta_\ell(\theta),$$

with

$$\beta_\ell(\theta) = \frac{(2\theta-1)^{\ell+1}-(-1)^{\ell+1}}{2^{\ell+1}(\ell+1)!}. \tag{6}$$

Letting $Q_{i+\theta}$ denote the approximation of $\bar{u}(x_{i+\theta})$, we obtain

$$Q_{i+\theta} := \sum_{\ell=0}^{k}(\Delta x)^\ell\left(\alpha_\ell(\theta)R_i^{(\ell)} + \beta_\ell(\theta)R_{i+1}^{(\ell)}\right). \tag{7}$$

Here, we note that $\alpha_\ell(\theta)$ and $\beta_\ell(\theta)$ satisfy the following relations:

- If $\ell = 2n$, $0 \le n$, is a even number

$$\alpha_\ell(\theta) + \beta_\ell(\theta) = \frac{1}{(2n+1)!}\left(\frac{1}{2}\right)^{2n}. \tag{8}$$

- If $\ell = 2n+1$, $0 \le n$, is an odd number

$$\alpha_\ell(\theta) + \beta_\ell(\theta) = 0. \tag{9}$$

We list the explicit form of $\alpha_\ell(\theta)$ and $\beta_\ell(\theta)$ for $\ell = 0, 1, 2$:

$$\begin{aligned} &\alpha_0(\theta) = 1-\theta, \quad \alpha_1(\theta) = \frac{\theta(1-\theta)}{2}, \quad \alpha_2(\theta) = \frac{1-q(\theta)}{24} \\ &\beta_0(\theta) = \theta, \quad \beta_1(\theta) = -\frac{\theta(1-\theta)}{2}, \quad \beta_2(\theta) = \frac{q(\theta)}{24}, \end{aligned} \tag{10}$$

where $q(\theta) = 3\theta - 6\theta^2 + 4\theta^3$, for $\theta \in [0, 1)$.

Remark 2.1 *(Finite difference framework).* Given a smooth function u, there exists a function $\hat{u}$ whose sliding average recovers the value of u:

$$u(x) = \frac{1}{\Delta x}\int_{x-\Delta x/2}^{x+\Delta x/2}\hat{u}(y)\,dy.$$

Since we can look for a basic reconstruction $R = \sum_i R_i(x)\chi_i(x)$ with R_i satisfying

$$\frac{1}{\Delta x}\int_{x_i-\Delta x/2}^{x_i+\Delta x/2} R(y)\,dy = u(x_i),$$

our reconstruction can be also used in the point-wise framework (see [5]). In view of this, we will apply it to the construction of semi-Lagrangian schemes in the finite difference framework.

2.1. General properties

In this section, we provide several properties of the reconstruction (7) such as accuracy, conservation and consistency with the classical interpolation by making a suitable choice of $R_i^{(\ell)}$ in the reconstruction.

Recalling the assumption (1), we have a function $R(x)$ which approximates point values of u and our goal is to approximate the sliding average function $\bar{u}$ with our reconstruction (7). Before checking the accuracy order, we note that the cell average function $\bar{u}(x)$ can be expressed in terms of derivatives of function $u(x)$:

$$\bar{u}(x) = \frac{1}{\Delta x}\int_{x-\Delta x/2}^{x+\Delta x/2} u(y)\,dy = \frac{1}{\Delta x}\int_{x-\Delta x/2}^{x+\Delta x/2}\sum_{\ell=0}^{\infty}\frac{u^{(\ell)}(x)}{\ell!}(y-x)^{\ell}\,dy = \sum_{\ell=\text{even}}^{\infty}(\Delta x)^{\ell}\,u^{(\ell)}(x)\frac{1}{(\ell+1)!}\left(\frac{1}{2}\right)^{\ell}. \tag{11}$$

Inserting $x = x_{i+\theta}$ into (11), we obtain

$$\bar{u}(x_{i+\theta}) = \sum_{\ell=\text{even}}^{\infty}(\Delta x)^{\ell}\,u^{(\ell)}(x_{i+\theta})\frac{1}{(\ell+1)!}\left(\frac{1}{2}\right)^{\ell} = u^{(0)}(x_{i+\theta}) + \frac{(\Delta x)^2}{24}u^{(2)}(x_{i+\theta}) + \frac{(\Delta x)^4}{1920}u^{(4)}(x_{i+\theta}) + \cdots.$$

With this formula, in the following proposition, we provide a sufficient condition for a polynomial reconstruction $Q_{i+\theta}$ to be a $(k+2)$-th order accurate approximation of $\bar{u}(x+\theta)$ for $\theta \in [0,1)$.

Proposition 2.1. *Let $k \geq 0$ be an even integer, $R_i \in \mathbb{P}^k$ be given by (4), and u be a smooth function $u : \mathbb{R} \in \mathbb{R}$. Suppose we have a piecewise polynomial $R(x) = \sum_i R_i(x)\chi_i(x)$, which satisfies*

$$\begin{aligned} u_i^{(\ell)} &= R_i^{(\ell)} + \mathcal{O}(\Delta x^{k+2-\ell}), \quad 0 \leq \ell \leq k, \text{ whenever } \ell \text{ is an even integer} \\ u_i^{(\ell)} - u_{i+1}^{(\ell)} &= R_i^{(\ell)} - R_{i+1}^{(\ell)} + \mathcal{O}(\Delta x^{k+2-\ell}), \quad 0 \leq \ell < k, \text{ whenever } \ell \text{ is an odd integer.} \end{aligned} \tag{12}$$

Then, the reconstruction $Q_{i+\theta}$ gives a $(k+2)$-th order approximation of the sliding average $\bar{u}(x_{i+\theta})$ for any $\theta \in [0,1)$.

Proof. For detailed proof, see Appendix A. □

Remark 2.2.

1. The reconstruction $Q_{i+\theta}$ approximates $\bar{u}(x_{i+\theta})$ on the basis of cell average values $\{\bar{u}_i\}_{i\in\mathcal{I}}$. Similarly, we can extend the idea of reconstruction to the framework of point values, which are used in conservative finite difference methods in section 4.
2. We also note that the second condition in (12) can be easily satisfied. Let $k \geq 0$ be an even integer, and consider a function $u(x) \in C^{k+2}(\mathbb{R})$, and its primitive function $U(x) := \int_{-\infty}^{x} u(y)\,dy \in C^{k+3}(\mathbb{R})$. We first look for a polynomial $P_i(x) \in \mathbb{P}^{k+1}$ such that

$$P_i(x_{i-\frac{1}{2}+j}) = U(x_{i-\frac{1}{2}+j}), \quad j = -r, \cdots, s+1, \quad r+s = k.$$

Then, the classical interpolation theory gives

$$U(x) - P_i(x) = \frac{1}{(k+2)!}U^{(k+2)}(\xi_i)\prod_{j=-r}^{s+1}(x - x_{i-\frac{1}{2}+j}), \quad \xi_i \in (x_{i-\frac{1}{2}-r}, x_{i+\frac{1}{2}+s}),$$

its first order derivative $p_i(x) \equiv P_i'(x) \in \mathbb{P}^k$ interpolates u in the sense of cell-average:

$$\frac{1}{\Delta x}\int_{x_{i+j}-\Delta x/2}^{x_{i+j}+\Delta x/2} p_i(y)\,dy = \bar{u}_{i+j}, \quad j = -r, \cdots, s,$$

and, for $0 \leq \ell \leq k$, its $(\ell+1)$-th derivative $p_i^{(\ell)}(x) \equiv P_i^{(\ell+1)}(x) \in \mathbb{P}^{k-\ell}$ satisfies

$$u^{(\ell)}(x) - p_i^{(\ell)}(x) = U^{(\ell+1)}(x) - P_i^{(\ell+1)}(x) = \frac{1}{(k+2)!}U^{(k+2)}(\xi_i)\frac{d^{\ell+1}}{dx^{\ell+1}}\left(\prod_{j=-r}^{s+1}(x - x_{i-\frac{1}{2}+j})\right). \tag{13}$$

Similarly, we can find polynomials $p_{i+1}(x) \in \mathbb{P}^k$ and $P_{i+1}(x) \in \mathbb{P}^{k+1}$ such that

$$\begin{aligned} u^{(\ell)}(x+\Delta x) - p_{i+1}^{(\ell)}(x+\Delta x) &= U^{(\ell+1)}(x+\Delta x) - P_{i+1}^{(\ell+1)}(x+\Delta x) \\ &= \frac{1}{(k+2)!}U^{(k+2)}(\xi_{i+1})\frac{d^{\ell+1}}{dx^{\ell+1}}\left(\prod_{j=-r}^{s+1}(x+\Delta x - x_{i+1-\frac{1}{2}+j})\right), \end{aligned}$$

where $\xi_{i+1} \in (x_{i+\frac{1}{2}-r}, x_{i+\frac{3}{2}+s})$. Then, the relation $U^{(k+2)}(\xi_i) - U^{(k+2)}(\xi_{i+1}) = \mathcal{O}(\Delta x)$, gives

$$\left(u^{(\ell)}(x_i) - p_i^{(\ell)}(x_i)\right) - \left(u^{(\ell)}(x_{i+1}) - p_{i+1}^{(\ell)}(x_{i+1})\right)$$
$$= \frac{1}{(k+2)!}\left(U^{(k+2)}(\xi_i) - U^{(k+2)}(\xi_{i+1})\right)\left\{\frac{d^\ell}{dx^\ell}\left(\prod_{j=-r}^{s+1}(x - x_{i-\frac{1}{2}+j})\right)\right\}_{x=x_i} = \mathcal{O}\left((\Delta x)^{k+2-\ell}\right).$$

3. If $R_i^{(\ell)}$ can be represented with a Lipschitz function F_ℓ:

$$R_i^{(\ell)} = F_\ell\left(\bar{u}_{i-r}, \cdots, \bar{u}_{i+s}\right)$$

which satisfies

$$F_\ell\left(\bar{u}_{i-r}, \cdots, \bar{u}_{i+s}\right) - u^{(\ell)}(x_i) = \mathcal{O}\left((\Delta x)^{k+1-\ell}\right),$$

the condition (12) is also satisfied. For more details, we refer to Appendix B.

In Proposition 2.1, we see that the choice of an even integer $k \geq 0$ leads to the improvement of accuracy. In such a case, we show that the reconstruction $Q_{i+\theta}$ based on linear weights coincides with the classical interpolation.

Proposition 2.2. *Let $k \geq 0$ be an even integer with $k = 2r$. For each $i \in \mathcal{I}$, assume that we have a basic reconstruction $R_i(x) \in \mathbb{P}^k$, which is a polynomial of degree k in (4) and interpolates the function u in the sense of cell averages:*

$$\frac{1}{\Delta x}\int_{x_{i+j-\frac{1}{2}}}^{x_{i+j+\frac{1}{2}}} R_i(x)\,dx = \bar{u}_{i+j}, \quad -r \leq j \leq r, \tag{14}$$

with a symmetric stencil $S_i := \{i-r, i-r+1, \cdots, i+r\}$. Then, the reconstruction $Q_{i+\theta}$ in (7) based on R_i and R_{i+1}, is the Lagrange polynomial $L(x)$ that interpolates $\bar{u}_{i+j}$, for $-r \leq j \leq r+1$, where $x = x_i + \theta\Delta x$ and $\theta \in [0, 1)$.

The proof is based on the observation that interpolation in the sense of the cell averages is equivalent to point-wise interpolation of sliding averages at cell center, which in turn, is equivalent to point-wise interpolation of primitive function at cell edges. The proof is provided in [25].

Remark 2.3. For $k = 0$, the only possible choice is to set $R_i(x) \equiv \bar{u}_i$ and the resulting reconstruction $Q_{i+\theta}$ reduces to the linear interpolation constructed from two points $\bar{u}_i$ and $\bar{u}_{i+1}$.

In the following proposition, we show that total mass is preserved for any θ-shifted summation, $\theta \in [0, 1)$.

Proposition 2.3. *Assume that $R_i(x)$ of the form (4) are polynomials satisfying*

$$\frac{1}{\Delta x}\int_{x_{i-\frac{1}{2}}}^{x_{i+\frac{1}{2}}} R_i(x)\,dx = \bar{u}_i, \quad i \in \mathcal{I}, \tag{15}$$

and $Q_{i+\theta}$ is constructed according to (7). Then, for periodic functions $\bar{u}(x)$ with period $L = N\Delta x$, $N \in \mathbb{N}$

$$\sum_{i=1}^{N} Q_{i+\theta} = \sum_{i=1}^{N} \bar{u}_i, \tag{16}$$

for any $\theta \in [0, 1)$.

Proof. Since θ does not depend on i,

$$\sum_{i=1}^{N} Q_{i+\theta} = \sum_{i=1}^{N}\left(\frac{1}{\Delta x}\int_{x_{i-\frac{1}{2}+\theta}}^{x_{i+\frac{1}{2}}} R_i(x)\,dx + \frac{1}{\Delta x}\int_{x_{i+\frac{1}{2}}}^{x_{i+\frac{1}{2}+\theta}} R_{i+1}(x)\,dx\right)$$

Table 1
Relative conservation errors (19) of the reconstruction for $\bar{u}_1$ (17) and $\bar{u}_2$ (18). Numerical solutions are obtained with $N_x = 40$.

Reconstruction	$\bar{u}_1$ in (17)	$\bar{u}_2$ in (18)
Q-CWENO23	4.4409e-16	7.7716e-16
GWENO34	1.1102e-15	2.8523e-05

$$= \sum_{i=1}^{N} \left(\frac{1}{\Delta x} \int_{x_{i-\frac{1}{2}+\theta}}^{x_{i+\frac{1}{2}}} R_i(x)\,dx + \frac{1}{\Delta x} \int_{x_{i-\frac{1}{2}}}^{x_{i-\frac{1}{2}+\theta}} R_i(x)\,dx \right)$$

$$= \sum_{i=1}^{N} \frac{1}{\Delta x} \int_{x_{i-\frac{1}{2}}}^{x_{i+\frac{1}{2}}} R_i(x)\,dx = \sum_{i=1}^{N} \bar{u}_i.$$

Here we used the periodicity to write the second line and (15) for the last line. □

Remark 2.4. We remark that this summation preserving property can be useful when our reconstruction is applied to the semi-Lagrangian treatment of a constant convection term, where characteristic curves are given by parallel lines for each grid point. In such cases, the proposed reconstruction attains conservation at a discrete level, hence it can be applied to the simulation of physical models satisfying this conservation property. Considerable examples are the BGK type models of the Boltzmann equation of rarefied gas dynamics. We can also apply this to the splitting method for the Vlasov-Poisson system in plasma physics. These problems will be considered in the second part of this paper.

In the following section, we will show that our reconstruction (7) inherits some properties of the basic reconstruction $R_i(x)$ such as non-oscillatory property and positivity.

2.2. Choice of the basic reconstruction R

2.2.1. Non-oscillatory property

Most common reconstructions adopted in the derivation of high resolution shock capturing schemes are at the same time conservative and (essentially) non-oscillatory. The WENO methodology [5], for example, satisfies such properties and is widely adopted. Using it as a basic reconstruction R, the resulting sliding average Q based on (7) will be smoother than R, and will inherit its non-oscillatory property. Throughout this paper, our particular choice of R will be one of such WENO methodology called CWENO. For reader's convenience, we illustrate CWENO23 [13] and CWENO35 [9] reconstructions in Appendix C.

Now we compare the proposed conservative reconstruction (C.3) using CWENO23 [14], which we call Q-CWENO23, with a generalized WENO reconstruction originally introduced in [6] in the context of semi-Lagrangian method, that we call GWENO. Here we use GWENO34 obtained with four points, which achieves fourth order accuracy in the smooth solution. Both reconstructions produce non-oscillatory solutions. If a function $\bar{u}$ is sufficiently smooth, then conservation errors in the GWENO reconstruction will be negligible, however, if the function changes abruptly, then GWENO may suffer from noticeable conservation errors. To show this, we consider two examples:

$$\bar{u}_1(x) = 1 + \frac{1}{2}\sin(4\pi x), \quad -1 \le x < 1, \tag{17}$$

$$\bar{u}_2(x) = 2 + \exp\left(-100\left(\frac{\sin(\pi x/2)}{\pi/2}\right)^2\right)\sin(\pi x) + 0.1\cos(\pi x) \quad -1 \le x < 1. \tag{18}$$

We assumed periodicity on the boundary condition for both functions. In order to clarify the difference between solutions, in Table 1, we report the maximal relative conservation errors between the summation of reconstructed points $Q_{i+\theta}$ and that of given points $\bar{u}_\ell(x_i)$, $\ell = 1, 2$, over $\theta = 0, 0.001, \ldots, 0.999$ using the following measure:

$$Err_\ell = \frac{max_\theta \left|\sum_i Q_{i+\theta} - \sum_i \bar{u}_\ell(x_i)\right|}{\sum_i \bar{u}_\ell(x_i)}, \quad \ell = 1, 2. \tag{19}$$

From the Table 1, we conclude that Q-CWENO23 recovers the reference summation of $\bar{u}_\ell(x_i)$ for any values of $\theta \in [0, 1)$. The errors for Q-CWENO23 and GWENO34 are both within machine precision for the smooth function $\bar{u}_1$. In this case, the two reconstructions almost coincides the standard Lagrangian interpolation which is conservative. When the function is not smooth as in $\bar{u}_2$, Q-CWENO23 is still fully conservative within machine precision, hence it verifies Proposition 2.3. Numerical experiments in which conservation is relevant will be discussed in section 5.

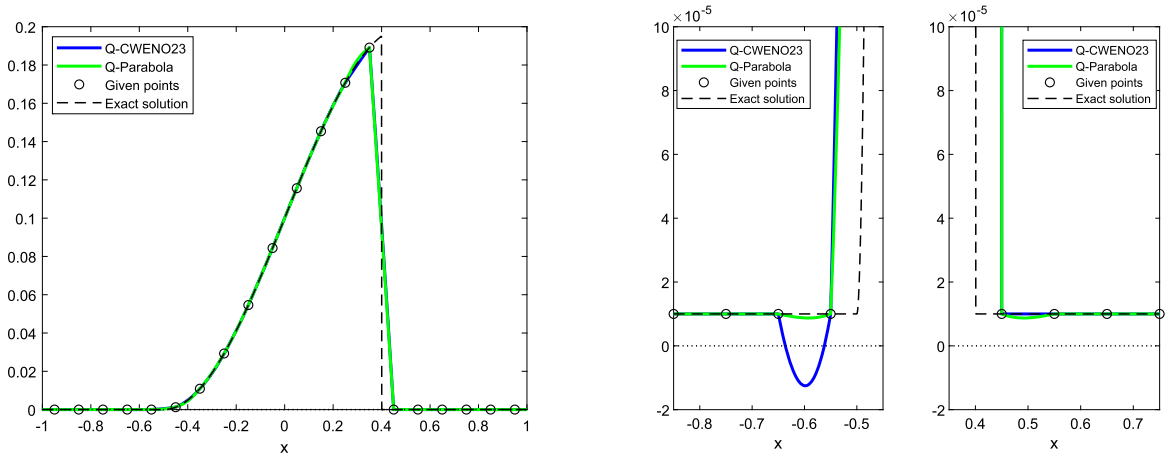

(a) Comparison of g given by (20) and its reconstructions.

(b) Comparison of g given by (20) and its reconstructions on $[-0.85, -0.45]$ and $[0.35, 0.75]$.

Fig. 2. Comparison of reconstructions between Q-Parabola and Q-CWENO23. Dashed lines are exact solutions $g(x)$ and black circles are given values on grid points of $g(x)$ given in (20).

2.2.2. Positivity preserving property

In several circumstances the solution one is looking for is a non-negative function. This is the case, for example, of distribution function in kinetic equations. In such cases it may be important to preserve at a discrete level the positivity of the solution. Standard piecewise polynomial reconstructions (linear reconstructions) do not preserve positivity, however several techniques exist in the literature that can be adopted to ensure positivity in the reconstruction ([17,18]). Here we remark that if the basic reconstruction R is positive preserving, then the sliding average of R will provide a conservative and positivity preserving reconstruction. Given a non-negative basic reconstructions $R_i(x) \geq 0$, obtained from positive cell averages $\bar{u}_i > 0 \; \forall i$, the positivity of the reconstruction (7) directly follows from (2). Here we verify this with a numerical example. Let us consider a basic reconstruction R_i, obtained by the *Positive Flux Conservative* (PFC) technique in [20]. The technique has been proposed to bound the numerical solution between zero and a prescribed maximum value. Hereafter we denote by Q-Parabola the reconstruction (7) based on this. In Fig. 2, we compare Q-Parabola with Q-CWENO23 reconstructions. For this, we consider a function on the periodic domain $[-1, 1]$:

$$g(x) = \begin{cases} 10^{-5} + 0.1\,(1 + \sin(\pi x))\,, & -0.5 \leq x \leq 0.4 \\ 10^{-5}, & \text{otherwise} \end{cases} . \tag{20}$$

In Fig. 2a and 2b, the difference between two reconstructions appears near $[-0.65, -0.55]$ and $[0.45, 0.55]$. In case of Q-Parabola, the use of positive limiter always guarantees positive reconstructions for any $x \in [-1, 1]$, while very small oscillations appear near discontinuities. On the other hand, although Q-CWENO23 always prevents spurious oscillation, negative solutions may occur depending on the choice of ϵ used for non-linear weights (C.2). In this case, we took $\epsilon = 10^{-6}$, and Eq. (C.2) of CWENO23 returns weights very close to the linear ones on the cell $[-0.6, -0.5]$, which gives negative values on the interval $[-0.65, -0.55]$. We remark that if CWENO23 reconstructions give linear polynomials on two consecutive cells, the corresponding reconstruction (7) is to be positive between the two cell centers. Consequently, the suitable choice of ϵ can enable Q-CWENO23 to avoid both negative reconstructions and spurious oscillations. Other possible ways to guarantee the positivity of basic reconstructions are to adopt a linear scaling approach [26–28] or use positive limiters [29,21].

Remark 2.5. We remark that both WENO and CWENO reconstructions and PFC satisfy condition (15) required in Proposition 2.3. Therefore, the Q reconstruction (7) based on such reconstructions satisfy the conservation property (16).

3. Conservative reconstruction in 2D

In this section, we introduce the conservative reconstruction technique in two space dimensions, following the one adopted in the previous section. Let $u : \mathbb{R}^2 \to \mathbb{R}$ be a smooth function and $\bar{u} : \mathbb{R}^2 \to \mathbb{R}$ be a corresponding sliding average function:

$$\bar{u}(x, y) = \frac{1}{\Delta x \Delta y} \int_{y-\Delta y/2}^{y+\Delta y/2} \int_{x-\Delta x/2}^{x+\Delta x/2} u(x, y)\, dx\, dy.$$

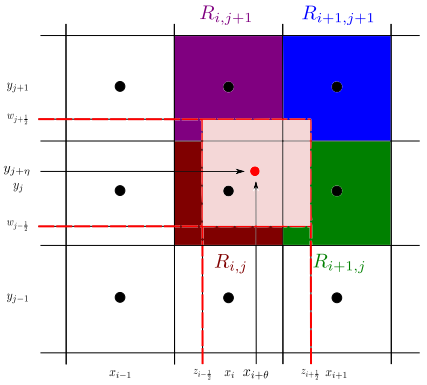

Fig. 3. Description of two-dimensional conservative reconstruction.

Given cell averages on grid points,

$$\frac{1}{\Delta x\Delta y}\int_{I_{i,j}} u(x)\,dx = \bar{u}_{i,j}, \quad I_{i,j} = [x_{i-\frac{1}{2}}, x_{i+\frac{1}{2}}] \times [y_{j-\frac{1}{2}}, y_{j+\frac{1}{2}}],$$

for each $(i, j) \in \mathcal{I}$, our goal is to approximate the function $\bar{u}(x, y)$. Assume we have a piecewise polynomial reconstruction $R(x, y) = \sum_{i,j} R_{i,j}(x, y)\chi_{i,j}(x, y)$, for $(i, j) \in \mathcal{I}$, where $\chi_{i,j}(x, y)$ is the characteristic function of cell $I_{i,j}$ and each $R_{i,j}(x, y)$ denotes a polynomial of degree k and has the following properties:

1. It is high order accurate in the approximation of $u(x, y)$:
$$u(x, y) = R_{i,j}(x, y) + \mathcal{O}\left(h^{k+1}\right), \quad (x, y) \in I_{i,j}, \tag{21}$$
where $\Delta x, \Delta y = \mathcal{O}(h)$.
2. It is conservative in the sense of cell averages:
$$\frac{1}{\Delta x\Delta y}\int_{y_{j-\frac{1}{2}}}^{y_{j+\frac{1}{2}}}\int_{x_{i-\frac{1}{2}}}^{x_{i+\frac{1}{2}}} R_{i,j}(x, y)\,dx\,dy = \bar{u}_{i,j}.$$

We start from a polynomial of degree k, $R_{i,j}(x, y)$:

$$R_{i,j}(x, y) = \sum_{|\ell|=0}^{k} \frac{R_{i,j}^{(\ell)}}{\ell_1!\ell_2!}(x - x_i)^{\ell_1}(y - y_j)^{\ell_2}, \tag{22}$$

where we use a multi index $\ell = (\ell_1, \ell_2)$. Consider a cell $I_{i,j}^{\theta,\eta}$ whose center is $(x_{i+\theta}, y_{j+\eta})$ for some $\theta, \eta \in [0, 1)$. In Fig. 3, we note that $(x_{i+\theta}, y_{j+\eta})$ lies inside one of $I_{i,j}, I_{i+1,j}, I_{i,j+1}, I_{i+1,j+1}$. Let us denote a cell $I_{i+\theta,j+\eta} := [z_{i-\frac{1}{2}}, z_{i+\frac{1}{2}}] \times [w_{j-\frac{1}{2}}, w_{j+\frac{1}{2}}]$ and a point $(x_{i+\theta}, y_{j+\eta}) := (x_i + \theta\Delta x, y_j + \eta\Delta y)$. Now, we approximate $\bar{u}(x_{i+\theta}, y_{j+\eta})$ by

$$\begin{aligned}
\bar{u}(x_{i+\theta}, y_{j+\eta}) &\approx \frac{1}{\Delta x\Delta y}\int_{w_{j-\frac{1}{2}}}^{w_{j+\frac{1}{2}}}\int_{z_{i-\frac{1}{2}}}^{z_{i+\frac{1}{2}}} R(x, y)\,dx\,dy \\
&= \frac{1}{\Delta x\Delta y}\int_{w_{j-\frac{1}{2}}}^{y_{j+\frac{1}{2}}}\int_{z_{i-\frac{1}{2}}}^{x_{i+\frac{1}{2}}} R_{i,j}(x, y)\,dx\,dy + \frac{1}{\Delta x\Delta y}\int_{w_{j-\frac{1}{2}}}^{y_{j+\frac{1}{2}}}\int_{x_{i+\frac{1}{2}}}^{z_{i+\frac{1}{2}}} R_{i+1,j}(x, y)\,dx\,dy \\
&+ \frac{1}{\Delta x\Delta y}\int_{y_{j+\frac{1}{2}}}^{w_{j+\frac{1}{2}}}\int_{z_{i-\frac{1}{2}}}^{x_{i+\frac{1}{2}}} R_{i,j+1}(x, y)\,dx\,dy + \frac{1}{\Delta x\Delta y}\int_{y_{j+\frac{1}{2}}}^{w_{j+\frac{1}{2}}}\int_{x_{i+\frac{1}{2}}}^{z_{i+\frac{1}{2}}} R_{i+1,j+1}(x, y)\,dx\,dy.
\end{aligned}$$

The first integral becomes

$$\begin{aligned}\frac{1}{\Delta x\Delta y}\int_{w_{j-\frac{1}{2}}}^{y_{j+\frac{1}{2}}}\int_{z_{i-\frac{1}{2}}}^{x_{i+\frac{1}{2}}} R_{i,j}(x,y)\,dxdy &= \frac{1}{\Delta x\Delta y}\sum_{|\ell|=0}^{k} R_{i,j}^{(\ell)}\int_{y_{j-\frac{1}{2}+\eta}}^{y_{j+\frac{1}{2}}}\int_{x_{i-\frac{1}{2}+\theta}}^{x_{i+\frac{1}{2}}}\frac{1}{\ell_1!\ell_2!}(x-x_i)^{\ell_1}(y-y_j)^{\ell_2}\,dxdy\\ &= \sum_{|\ell|=0}^{k} R_{i,j}^{(\ell)}\left(\frac{1}{\Delta x}\int_{x_{i-\frac{1}{2}+\theta}}^{x_{i+\frac{1}{2}}}\frac{(x-x_i)^{\ell_1}}{\ell_1!}\,dx\right)\left(\frac{1}{\Delta y}\int_{y_{j-\frac{1}{2}+\eta}}^{y_{j+\frac{1}{2}}}\frac{(y-y_j)^{\ell_2}}{\ell_2!}\,dy\right)\\ &= \sum_{|\ell|=0}^{k}(\Delta)^{\ell}\alpha_{\ell_1}(\theta)\alpha_{\ell_2}(\eta)R_{i,j}^{(\ell)}\end{aligned}$$

where $(\Delta)^{\ell}=(\Delta x)^{\ell_1}(\Delta y)^{\ell_2}$. Similarly, we obtain

$$\begin{aligned}\frac{1}{\Delta x\Delta y}\int_{w_{j-\frac{1}{2}}}^{y_{j+\frac{1}{2}}}\int_{x_{i+\frac{1}{2}}}^{z_{i+\frac{1}{2}}} R_{i+1,j}(x,y)\,dxdy &= \sum_{|\ell|=0}^{k}(\Delta)^{\ell}\beta_{\ell_1}(\theta)\alpha_{\ell_2}(\eta)R_{i+1,j}^{(\ell)},\\ \frac{1}{\Delta x\Delta y}\int_{y_{j+\frac{1}{2}}}^{w_{j+\frac{1}{2}}}\int_{z_{i-\frac{1}{2}}}^{x_{i+\frac{1}{2}}} R_{i,j+1}(x,y)\,dxdy &= \sum_{|\ell|=0}^{k}(\Delta)^{\ell}\alpha_{\ell_1}(\theta)\beta_{\ell_2}(\eta)R_{i,j+1}^{(\ell)},\\ \frac{1}{\Delta x\Delta y}\int_{y_{j+\frac{1}{2}}}^{w_{j+\frac{1}{2}}}\int_{x_{i+\frac{1}{2}}}^{z_{i+\frac{1}{2}}} R_{i+1,j+1}(x,y)\,dxdy &= \sum_{|\ell|=0}^{k}(\Delta)^{\ell}\beta_{\ell_1}(\theta)\beta_{\ell_2}(\eta)R_{i+1,j+1}^{(\ell)}.\end{aligned}$$

Denoting the approximation of $\bar{u}(x_{i+\theta},y_{j+\theta})$ by $Q_{i+\theta,j+\eta}$, we write it as

$$\begin{aligned}Q_{i+\theta,j+\eta}=\sum_{|\ell|=0}^{k}(\Delta)^{\ell}\Big(&\alpha_{\ell_1}(\theta)\alpha_{\ell_2}(\eta)R_{i,j}^{(\ell)}+\beta_{\ell_1}(\theta)\alpha_{\ell_2}(\eta)R_{i+1,j}^{(\ell)}\\ &+\alpha_{\ell_1}(\theta)\beta_{\ell_2}(\eta)R_{i,j+1}^{(\ell)}+\beta_{\ell_1}(\theta)\beta_{\ell_2}(\eta)R_{i+1,j+1}^{(\ell)}\Big),\end{aligned}\tag{23}$$

where the explicit forms of $\alpha_{\ell_1}(\theta)$, $\alpha_{\ell_2}(\eta)$, $\beta_{\ell_1}(\theta)$, $\beta_{\ell_2}(\eta)$ are given in (5) and (6).

3.1. General properties

In the following proposition, as in Proposition 2.3, we show that the approximation $Q_{i+\theta,j+\eta}$ is of order $(k+2)$ of accuracy for an even integer $k\geq 0$. For simplicity, we assume $\Delta x,\Delta y=h>0$.

Proposition 3.1. *Let $k\geq 0$ be an even integer and u be smooth enough so that a piecewise polynomial $R(x,y)=\sum_{i,j}R_{i,j}(x,y)\chi_{i,j}(x,y)$ satisfies*

$$\begin{aligned}u_{i,j}^{(\ell)}&=R_{i,j}^{(\ell)}+\mathcal{O}(h^{k+2-|\ell|}),\quad \ell\in A\\ u_{i,j}^{(\ell)}-u_{i+1,j}^{(\ell)}&=R_{i,j}^{(\ell)}-R_{i+1,j}^{(\ell)}+\mathcal{O}(h^{k+2-|\ell|}),\quad \ell\in B\\ u_{i,j}^{(\ell)}-u_{i,j+1}^{(\ell)}&=R_{i,j}^{(\ell)}-R_{i,j+1}^{(\ell)}+\mathcal{O}(h^{k+2-|\ell|}),\quad \ell\in C\end{aligned}\tag{24}$$

where the set A, B and C are defined

$$\begin{aligned}A&=\{\ell:|\ell|=even,\quad 0\leq|\ell|\leq k\},\\ B&=\{\ell:\ell_1=odd,\quad \ell_2=even,\quad 0\leq|\ell|\leq k\},\\ C&=\{\ell:\ell_1=even,\quad \ell_2=odd,\quad 0\leq|\ell|\leq k\}.\end{aligned}\tag{25}$$

Then the reconstruction $Q_{i+\theta,j+\eta}$ gives a $(k+2)$-th-order approximation of sliding averages $\bar{u}_{i+\theta,j+\eta}$ for any $\theta,\eta\in[0,1)$.

Proof. For detailed proof, see Appendix D. □

The conservation property also holds in the 2D reconstruction (23):

Proposition 3.2. *Assume that $R_{i,j}(x, y)$ satisfies*

$$\frac{1}{\Delta x \Delta y} \int_{y_{j-\frac{1}{2}}}^{y_{j+\frac{1}{2}}} \int_{x_{i-\frac{1}{2}}}^{x_{i+\frac{1}{2}}} R_{i,j}(x, y)\, dx\, dy = \bar{u}_{i,j}, \quad (i, j) \in \mathcal{I}.$$

Then, for periodic functions $\bar{u}(x, y)$ with period $(L, L) = (Nh, Nh)$, $N \in \mathbb{N}$

$$\sum_{1 \le i,j \le N} Q_{i+\theta, j+\theta} = \sum_{1 \le i,j \le N} \bar{u}_{i,j},$$

for any $\theta, \eta \in [0, 1)$.

Proof. The proof is similar to the one-dimensional case. □

4. Semi-Lagrangian schemes for hyperbolic systems with relaxation

In this section we apply semi-Lagrangian methods based on the conservative reconstruction (7) and (23) to two semi-linear hyperbolic relaxation systems, namely, Xin-Jin system [30] and Broadwell model [31], where a relaxation parameter κ makes each system stiff as $\kappa \to 0$. In order to treat the stiffness, we use L-stable s-stage DIRK methods or BDF methods) [32]. Following conventional notation, we represent L-stable s-stage DIRK methods by Butcher's tables:

$$\begin{array}{c|c} c & A \\ \hline & b^T \end{array}$$

where $A = [a_{k\ell}]$ is a $s \times s$ lower triangle matrix such that $a_{k\ell} = 0$ for $\ell > k$, $c = (c_1, ..., c_s)^T$ and $b = (b_1, ..., b_s)^T$ are coefficient vectors. (For BDF based methods, we refer to Appendix E.1.) In the numerical tests for each order of accuracy, we will use the following high-order L-stable DIRK methods:

- second-order DIRK method (DIRK2) [33],

$$\begin{array}{c|cc} \alpha & \alpha & 0 \\ 1 & 1-\alpha & \alpha \\ \hline & 1-\alpha & \alpha \end{array}, \quad \alpha = 1 - \frac{\sqrt{2}}{2}. \tag{26}$$

- third-order DIRK method (DIRK43) [34],

$$\begin{array}{c|cccc} 0 & 0 & 0 & 0 & 0 \\ 2\gamma & \gamma & \gamma & 0 & 0 \\ c & c-\delta-\gamma & \delta & \gamma & 0 \\ 1 & 1-b_2-b_3-\gamma & b_2 & b_3 & \gamma \\ \hline & 1-b_2-b_3-\gamma & b_2 & b_3 & \gamma \end{array} \tag{27}$$

with $\gamma = \frac{1767732205903}{4055673282236}$, $c = \frac{3}{5}$, $b_2 = -\frac{4482444167858}{7529755066697}$, $b_3 = \frac{11266239266428}{11593286722821}$, $\delta = -\frac{640167445237}{6845629431997}$.

4.1. Xin-Jin relaxation system

Consider a simplified Xin-Jin relaxation system [30]:

$$\begin{aligned} &\frac{\partial u}{\partial t} + \sum_{i=1}^{d} \frac{\partial v}{\partial x_i} = 0, \\ &\frac{\partial v}{\partial t} + a^2 \sum_{i=1}^{d} \frac{\partial u}{\partial x_i} = \frac{1}{\kappa}(F(u) - v), \end{aligned} \tag{28}$$

where d denotes space dimension. When κ goes to zero, the solution in (28) converges to

$$\frac{\partial u}{\partial t}+\sum_{i=1}^{d}\frac{\partial F(u)}{\partial x_i}=0,\quad v=F(u), \tag{29}$$

provided that the subcharacteristic condition is satisfied, i.e., $\max_u |F'(u)| \le |a|$ (see [35]). For example, taking $F(u)=u^2/2$, the system (29) formally becomes the Burgers equation:

$$\frac{\partial u}{\partial t}+\sum_{i=1}^{d}u\frac{\partial u}{\partial x_i}=0,\quad v=\frac{u^2}{2}. \tag{30}$$

In this equation, shocks may appear in a finite time and we need to impose our scheme to be conservative to capture the positions of such shocks correctly. We treat this shock problem in section 5.

4.1.1. Semi-Lagrangian scheme for Xin-Jin relaxation system

Hereafter we fix $a=1$. Using $u-v=f$ and $u+v=g$, we rewrite (28) as

$$\begin{aligned}\frac{\partial f}{\partial t}-\sum_{i=1}^{d}\frac{\partial f}{\partial x_i}&=-\frac{1}{\kappa}\left[F\left(\frac{g+f}{2}\right)-\frac{g-f}{2}\right]\\ \frac{\partial g}{\partial t}+\sum_{i=1}^{d}\frac{\partial g}{\partial x_i}&=-\frac{1}{\kappa}\left[\frac{g-f}{2}-F\left(\frac{g+f}{2}\right)\right].\end{aligned} \tag{31}$$

Based on this, we consider its Lagrangian formulation:

$$\begin{aligned}\frac{df}{dt}(X_1(t),t)&=-\frac{1}{\kappa}\left[F\left(\frac{g+f}{2}\right)-\frac{g-f}{2}\right](X_1(t),t),\quad \frac{dX_1}{dt}=-\mathbb{1}\\ \frac{dg}{dt}(X_2(t),t)&=-\frac{1}{\kappa}\left[\frac{g-f}{2}-F\left(\frac{g+f}{2}\right)\right](X_2(t),t),\quad \frac{dX_2}{dt}=\mathbb{1},\end{aligned} \tag{32}$$

where $\mathbb{1}=(1,\cdots,1)\in\mathbb{N}^d$ and $X_1(t^{n+1})=X_2(t^{n+1})=x_i\in\mathbb{R}^d$.

To clarify high order methods for (32), we introduce the following notation:

- The ℓ-th stage values of f,g along the backward-characteristics which come from x_i with characteristic speed $-1,1$ at time $t^n+c_k\Delta t$:

  $$\tilde f_i^{(k,\ell)}\approx f(x_i+(c_k-c_\ell)\Delta t,t^n+c_\ell\Delta t),\quad \tilde g_i^{(k,\ell)}\approx f(x_i-(c_k-c_\ell)\Delta t,t^n+c_\ell\Delta t)$$

  where "$\approx$" implies the necessity of suitable reconstructions. We also denote k-th stage value of f,g on x_i by

  $$f_i^{(k)}=f(x_i,t^n+c_k\Delta t),\quad g_i^{(k)}=g(x_i,t^n+c_k\Delta t)$$

  for $1\le k\le s$ where $f_i^{(k)}=u_i^{(k)}-v_i^{(k)}$ and $g_i^{(k)}=u_i^{(k)}+v_i^{(k)}$.
- For $\ell=0$, we set $c_\ell=0$ hence

  $$\tilde f_i^{(k,0)}\approx f(x_i+c_k\Delta t,t^n),\quad \tilde g_i^{(k,0)}\approx g(x_i-c_k\Delta t,t^n). \tag{33}$$

- Define a RK flux function by $K_1:=F(u)-v$, $K_2:=-K_1$, then

  $$K_{i,j}^{(k,\ell)}\approx K_j(x_i-\lambda_j(c_k-c_\ell)\Delta t,t^n+c_\ell\Delta t),\quad j=1,2$$

  where $\lambda_1=-1,\lambda_2=1$ and $K_{i,j}^{(k)}=K_j(x_i,t^n+c_k\Delta t)$.

With these, we can represent a high order method compactly. Applying a L-stable s-stage DIRK method to system (32), we have k-stage values

$$\begin{aligned}f_i^{(k)}&=\tilde f_i^{(k,0)}-\frac{\Delta t}{\kappa}\sum_{\ell=1}^{k}a_{k\ell}K_{i,1}^{(k,\ell)},\\ g_i^{(k)}&=\tilde g_i^{(k,0)}-\frac{\Delta t}{\kappa}\sum_{\ell=1}^{k}a_{k\ell}K_{i,2}^{(k,\ell)},\end{aligned} \tag{34}$$

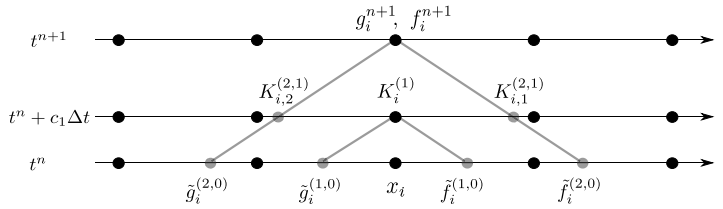

Fig. 4. DIRK2 based SL method for Xin-Jin model. Gray circles are points where reconstruction is required.

for $k = 1, \dots, s$. It is worth mentioning that each k-stage value can be computed in an explicit way. After summing and subtracting two equations in (34), we obtain

$$\begin{aligned} u_i^{(k)} &= \frac{\tilde{g}_i^{(k,0)} + \tilde{f}_i^{(k,0)}}{2} - \frac{\Delta t}{2\kappa} \sum_{\ell=1}^{k-1} a_{k\ell} \left(K_{i,1}^{(k,\ell)} + K_{i,2}^{(k,\ell)} \right), \\ v_i^{(k)} &= \frac{\tilde{g}_i^{(k,0)} - \tilde{f}_i^{(k,0)}}{2} - \frac{\Delta t}{2\kappa} \left(\sum_{\ell=1}^{k-1} a_{k\ell} \left(K_{i,2}^{(k,\ell)} - K_{i,1}^{(k,\ell)} \right) \right) + \frac{a_{kk}\Delta t}{\kappa} \left(F(u_i^{(k)}) - v_i^{(k)} \right). \end{aligned} \tag{35}$$

Here we first compute $u_i^{(k)}$, and use it to obtain $v_i^{(k)}$. Then, we recover the values of $f_i^{(k)}$ and $g_i^{(k)}$ using the relation:

$$f_i^{(k)} = u_i^{(k)} - v_i^{(k)}, \quad g_i^{(k)} = u_i^{(k)} + v_i^{(k)}.$$

Since we only consider stiffly accurate DIRK schemes, the s-stage values become the numerical solutions: $f_i^{n+1} = f_i^{(s)}$ and $g_i^{n+1} = g_i^{(s)}$. A schematic illustration of DIRK2 based scheme is given in Fig. 4. For any term where reconstruction is required, we use QCWENO reconstruction (7). In a similar manner, BDF based methods can be also devised. The details are described in Appendix E.1.

Remark 4.1. In case of the implicit Euler method for $s = 1$, by taking a limit $\kappa \to 0$ in (35) we obtain

$$u_i^{n+1} = \frac{\tilde{g}_i^{(1,0)} + \tilde{f}_i^{(1,0)}}{2}, \quad v_i^{n+1} = F(u_i^{n+1}), \tag{36}$$

for all $n \geq 0$ regardless of initial data. Now, we assume $\Delta t = \Delta x$, combine (36) with (33), and use the relations $u - v = f$ and $u + v = g$ to obtain

$$u_i^{n+1} = \frac{1}{2}\left(u_{i+1}^n + u_{i-1}^n\right) - \frac{1}{2}\left(F\left(u_{i+1}^n\right) - F\left(u_{i-1}^n\right)\right).$$

This is the Lax–Friedrichs method of the conservation law in (29) with $\Delta t = \Delta x$.

4.2. Broadwell model

Next example is the Broadwell model of kinetic theory [31]:

$$\begin{aligned} \partial_t f + \partial_x f &= \frac{1}{\kappa} Q \\ \partial_t g - \partial_x g &= \frac{1}{\kappa} Q \\ \partial_t h &= -\frac{1}{\kappa} Q, \end{aligned} \tag{37}$$

where $Q = h^2 - fg$. Introducing the fluid dynamic moment variables density ρ, momentum m, and velocity u and an additional variable z as follows:

$$\rho = f + 2h + g, \quad m = f - g, \quad z = f + g, \tag{38}$$

the system (37) can be rewritten as

$$\begin{aligned} &\partial_t \rho + \partial_x m = 0 \\ &\partial_t m + \partial_x z = 0 \\ &\partial_t z + \partial_x m = \frac{1}{2\kappa}\left(\rho^2 - 2\rho z + m^2\right). \end{aligned} \tag{39}$$

Note that the original variables can be recovered by

$$f = \frac{z+m}{2}, \quad g = \frac{z-m}{2}, \quad h = \frac{\rho - z}{2}.$$

As $\kappa \to 0$, one can see that z goes to a local equilibrium

$$z \to z_E(\rho, m) := \frac{1}{2\rho}\left(\rho^2 + m^2\right) = \frac{1}{2}\left(\rho + \rho u^2\right)$$

and the system (39) becomes the Euler equations:

$$\begin{aligned} &\partial_t \rho + \partial_x m = 0 \\ &\partial_t m + \partial_x \left(\frac{1}{2}\left(\rho + \rho u^2\right)\right) = 0. \end{aligned} \tag{40}$$

4.2.1. Semi-Lagrangian scheme for the Broadwell model

Here, we consider again DIRK methods based on Tables (26)-(27). The schemes are also explicitly solvable with algebraic computations. (For BDF based methods, see Appendix E.2.)

Let us denote k-th stage values by $f_i^{(k)}$, $g_i^{(k)}$, $h_i^{(k)}$, $1 \le k \le s$, and introduce the following notation:

$$\begin{aligned} &Q_i^{(k)} = (h_i^{(k)})^2 - f_i^{(k)} g_i^{(k)}, \\ &Q_{i,1}^{(k,\ell)} \approx Q\left(x_i - (c_k - c_\ell)\Delta t, t^n + c_\ell \Delta t\right), \quad Q_{i,2}^{(k,\ell)} \approx Q\left(x_i + (c_k - c_\ell)\Delta t, t^n + c_\ell \Delta t\right), \\ &f_i^{(k,\ell)} \approx f\left(x_i - (c_k - c_\ell)\Delta t, t^n + c_\ell \Delta t\right), \quad g_i^{(k,\ell)} \approx g\left(x_i - (c_k - c_\ell)\Delta t, t^n + c_\ell \Delta t\right). \end{aligned}$$

Here we also use the QCWENO reconstruction (7) for interpolation. Applying a s-stage DIRK method to (37), we can write k-th stage values in a compact form:

$$\begin{aligned} f_i^{(k)} &= F_i^{(k)} + \frac{a_{kk}\Delta t}{\kappa} Q_i^{(k)}, \quad F_i^{(k)} := f_i^{(k,0)} + \frac{\Delta t}{\kappa}\sum_{\ell=1}^{k-1} a_{k\ell} Q_{i,1}^{(k,\ell)} \\ g_i^{(k)} &= G_i^{(k)} + \frac{a_{kk}\Delta t}{\kappa} Q_i^{(k)}, \quad G_i^{(k)} := g_i^{(k,0)} + \frac{\Delta t}{\kappa}\sum_{\ell=1}^{k-1} a_{k\ell} Q_{i,2}^{(k,\ell)} \\ h_i^{(k)} &= H_i^{(k)} - \frac{a_{kk}\Delta t}{\kappa} Q_i^{(k)}, \quad H_i^{(k)} := h_i^{n} - \frac{\Delta t}{\kappa}\sum_{\ell=1}^{k-1} a_{k\ell} Q_i^{(\ell)}, \end{aligned} \tag{41}$$

for $k = 1, 2, \dots, s$. For explicit computation, we first need to compute $F_i^{(k)}$, $G_i^{(k)}$ and $H_i^{(k)}$ using (41). Then, we can update $h_i^{(k)}$, $f_i^{(k)}$ and $g_i^{(k)}$ as follows:

$$\begin{aligned} h_i^{(k)} &= \frac{a_{kk}\Delta t (H_i^{(k)} + F_i^{(k)})(H_i^{(k)} + G_i^{(k)}) + \kappa H_i^{(k)}}{a_{kk}\Delta t\left(G_i^{(k)} + 2H_i^{(k)} + F_i^{(k)}\right) + \kappa}, \\ f_i^{(k)} &= H_i^{(k)} + F_i^{(k)} - h_i^{(k)}, \qquad g_i^{(k)} = H_i^{(k)} + G_i^{(k)} - h_i^{(k)}. \end{aligned} \tag{42}$$

Here the SA property also implies $f_i^{n+1} = f_i^{(s)}$, $g_i^{n+1} = g_i^{(s)}$ and $h_i^{n+1} = h_i^{(s)}$.

Remark 4.2. In case $s = 1$ for implicit Euler method, under the assumption $\Delta t = \Delta x$, the relaxation limit $\kappa \to 0$ in (42) gives

$$\begin{aligned} h_i^{n+1} &= \frac{(h_i^n + f_{i-1}^n)(h_i^n + g_{i+1}^n)}{g_{i+1}^n + 2h_i^n + f_{i-1}^n}, \\ f_i^{n+1} &= h_i^n + f_i^{(1,0)} - h_i^{n+1}, \qquad g_i^{n+1} = h_i^n + g_i^{(1,0)} - h_i^{n+1}. \end{aligned} \tag{43}$$

This limiting scheme coincides with the relaxation scheme in [36] applied to the Broadwell model. Also, using the relation (38), we can rewrite it as follows:

$$\rho_i^{n+1} = \rho_i^n - \frac{1}{2}\left(m_{i+1}^n - m_{i-1}^n\right) + \frac{1}{2}\left(z_{i-1}^n - 2z_i^n + z_{i-1}^n\right),$$
$$m_i^{n+1} = \frac{1}{2}\left(m_{i+1}^n + m_{i-1}^n\right) - \frac{1}{2}\left(z_{i+1}^n - z_{i-1}^n\right),$$
$$z_i^{n+1} = \frac{(\rho_i^{n+1})^2 + (m_i^{n+1})^2}{2\rho_i^{n+1}}.$$

We note that the scheme projects numerical solutions to equilibrium after one time step.

5. Numerical tests

Our main interest is to confirm the performance of the proposed reconstruction in one and two dimensions. For numerical experiments, we consider the reconstruction (7) and (23) based on CWENO reconstructions. This section is divided into three parts: 1D Xin-Jin model (28), 1D Broadwell model (37) and 2D Xin-Jin model (28). For each system, we check the accuracy of the corresponding semi-Lagrangian schemes and consider the related shock problems which arise in the relaxation limit $\kappa \to 0$. Considering that the maximum characteristic speed of Broadwell model (37) and 1D Xin-Jin model (28) with $d = 1$ is given by 1, we set CFL$= \Delta t/\Delta x$ using uniform grid points based on Δx and Δt. For 2D Xin-Jin model (28) with $d = 2$, we use CFL$= \sqrt{2}\Delta t/\Delta x = \sqrt{2}\Delta t/\Delta y$.

5.1. 1D case for Xin-Jin model

Here tests are based on the numerical method in subsection 4.1.1. Note that we adopt $F(u) = u^2/2$.

5.1.1. Accuracy test

We take well-prepared initial data up to first order in κ [37]:

$$u_0(x) = 0.7 + 0.2\sin(\pi x), \quad v_0(x) = \frac{u_0^2(x)}{2} + \kappa\left(u_0^2(x) - 1\right)\partial_x u_0(x), \tag{44}$$

where periodic boundary conditions are imposed on $x \in [-1, 1]$. In the limit $\kappa \to 0$ with $F(u) = u^2/2$, system (28) becomes the Burgers equation where shock appears after the positive minimum time: $T_b := \inf_{u_0' < 0}\left\{-\frac{1}{u_0'(x)}\right\}$. In view of this, we take a final time as $T^f = 1$ which is less than the breaking time $T_b = 5/\pi \approx 1.5915$. In this test, we use several values of CFL$=\Delta t/\Delta x < 1$. We remark that the subcharacteristic condition $\max_u |F'(u)| < 1$ is always satisfied. In Table 2, we verify that a DIRK2 based method attains its desired accuracy between 2 and 3. In Fig. 5, DIRK43 based methods attain the desired accuracy between 3 and 5, while some order reduction appears in the intermediate regimes. We remark that the spatial errors are dominant for small CFL numbers, which make it easy to observe the order of spatial reconstructions. On the other hand, for large CFL numbers time errors become dominant, thus determining the numerical order of accuracy of the method.

5.1.2. Shock tests

To confirm the conservation property of the proposed reconstruction in shock problems, we here compare numerical solutions obtained by conservative semi-Lagrangian schemes with non-conservative ones.

• **Smooth initial data.** We first take a smooth initial data

$$u_0(x) = 0.7 + 0.2\sin(\pi x), \quad v_0(x) = \frac{u_0^2(x)}{2}, \tag{45}$$

where periodic boundary condition is imposed on $x \in [-1, 1]$. We use grid points of $N_x = 160$ up to final time $T^f = 4$. Each time step is taken by $\Delta t = \text{CFL}\Delta x$. For each time $t = t^n$, we compute the relative conservation error as

$$E_{con}^n := \frac{\left|\sum_i u_i^n - \sum_i u_i^0\right|}{\left|\sum_i u_i^0\right|}.$$

In Fig. 6, we compare the numerical solutions obtained from our reconstruction, linear interpolation (first order scheme), GWENO34 and GWENO46 [6] with the reference solution in [38]. We observe that the use of our reconstruction and linear interpolation leads to correct shock position. Also, the corresponding conservation errors show very small change as time flows. In contrast, conservation errors become bigger when we adopt GWENO34 and GWENO46 reconstructions after time $t = 1$, which give wrong shock positions. (See Fig. 6.)

Table 2
Accuracy test for 1D Xin-Jin model. Initial data is associated to (44). The errors and convergence rates are reported for DIRK2-QCWENO23.

	N_x-$2N_x$	$\kappa = 10^{-8}$		$\kappa = 10^{-6}$		$\kappa = 10^{-4}$		$\kappa = 10^{-2}$		$\kappa = 10^{-0}$	
		error	rate	error	rate	error	rate	error	rate	error	rate
$\frac{\Delta t}{\Delta x} = 0.1$	160-320	1.41e-05	2.99	1.41e-05	2.99	1.40e-05	2.99	7.40e-06	3.01	4.16e-06	3.00
	320-640	1.78e-06		1.78e-06		1.76e-06		9.22e-07		5.22e-07	
$\frac{\Delta t}{\Delta x} = 0.3$	160-320	1.27e-05	2.62	1.27e-05	2.62	1.22e-05	2.71	6.38e-06	2.77	3.44e-06	2.99
	320-640	2.07e-06		2.07e-06		1.86e-06		9.33e-07		4.34e-07	
$\frac{\Delta t}{\Delta x} = 0.5$	160-320	2.02e-05	1.99	2.02e-05	1.99	1.89e-05	2.09	7.79e-06	2.15	2.55e-06	2.96
	320-640	5.07e-06		5.06e-06		4.45e-06		1.75e-06		3.27e-07	
$\frac{\Delta t}{\Delta x} = 0.7$	160-320	4.02e-05	1.98	4.02e-05	1.98	3.82e-05	2.04	1.44e-05	2.04	1.62e-06	2.86
	320-640	1.02e-05		1.02e-05		9.28e-06		3.50e-06		2.24e-07	
$\frac{\Delta t}{\Delta x} = 0.9$	160-320	6.80e-05	1.99	6.80e-05	1.99	6.53e-05	2.04	2.48e-05	2.06	8.59e-07	2.35
	320-640	1.71e-05		1.71e-05		1.59e-05		5.94e-06		1.69e-07	

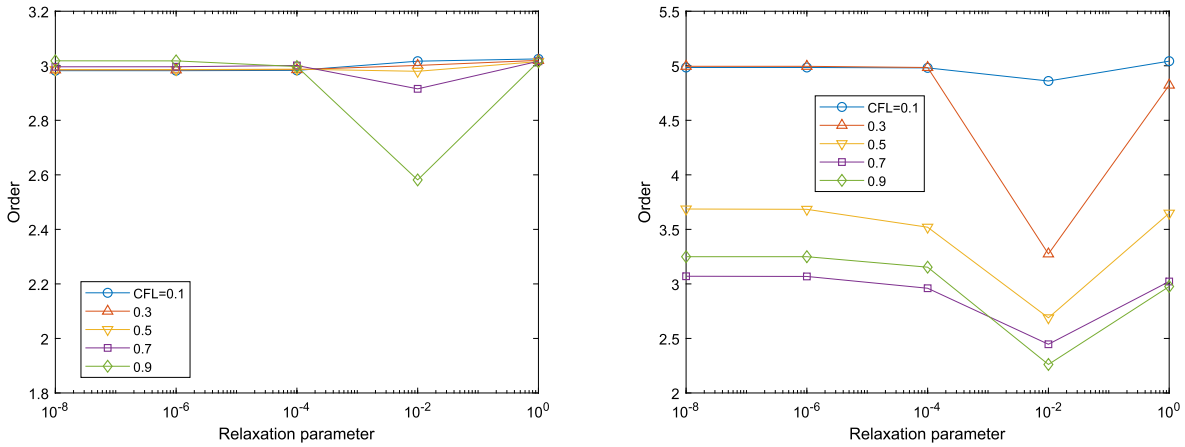

(a) DIRK43 - Q-CWENO23 (b) DIRK43 - Q-CWENO35

Fig. 5. Accuracy tests for 1D Xin-Jin model. Initial data is associated to (44). x-axis is for the relaxation parameter κ and y-axis is for order of accuracy based on $N_x = 160, 320, 640$.

- **Discontinuous initial data.** In this test, we again solve the system (28) with initial data

$$u_0(x) = \begin{cases} 0.9, & x \le 0 \\ 0, & x > 0 \end{cases}, \quad v_0(x) = \frac{u_0^2(x)}{2} \tag{46}$$

under freeflow boundary condition on $x \in [-1, 1]$ with grid points $N_x = 160$ up to final time $T^f = 1$. In this test, we compute the conservation error using

$$E_{con}^n := \frac{\left|\sum_i u_i^n \Delta x - 0.9 * (1 + st^n)\right|}{0.9},$$

where s is the speed of shock, which is given by $s = 0.45$.

We show our reconstruction can be more effective in capturing shock position. In Fig. 6, we again compare the numerical solutions for different reconstructions. As in the previous shock test, our reconstruction and linear interpolation show better performance in capturing shock position compared to GWENO34 and GWENO46 reconstructions.

Remark 5.1. In the section 5.1, we confirmed that for Xin-Jin model high-order DIRK based SL schemes work for all ranges of relaxation parameters. We also observed that, in the limit $\kappa \to 0$, oscillations appear near discontinuities for all high-order RK and BDF based SL schemes. To understand these phenomena, as a simple case, let us consider $F(u) = bu$ for $|b| < 1$. We will show that oscillation appears even after one step $t = t^1$ for arbitrary second order DIRK based SL schemes with linear interpolation (see Fig. 7). We use the Butcher's table given by

$$\begin{array}{c|cc} \alpha_1 & \alpha_1 & 0 \\ 1 & 1-\alpha_2 & \alpha_2 \\ \hline & 1-\alpha_2 & \alpha_2 \end{array}, \quad \alpha_2 = \frac{\frac{1}{2} - \alpha_1}{1 - \alpha_1}.$$

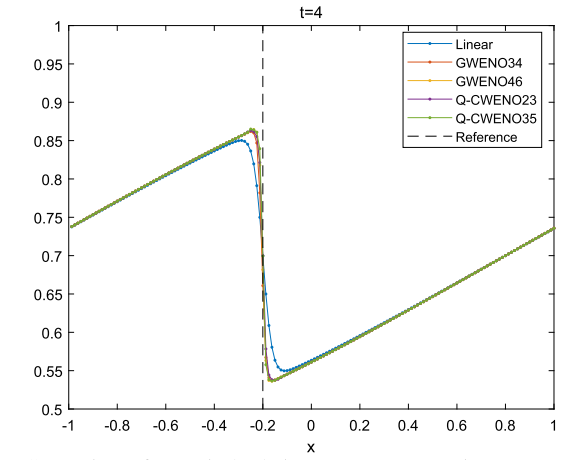

(a) Comparison of numerical solutions w.r.t. reconstruction at $x \in [-1, 1]$

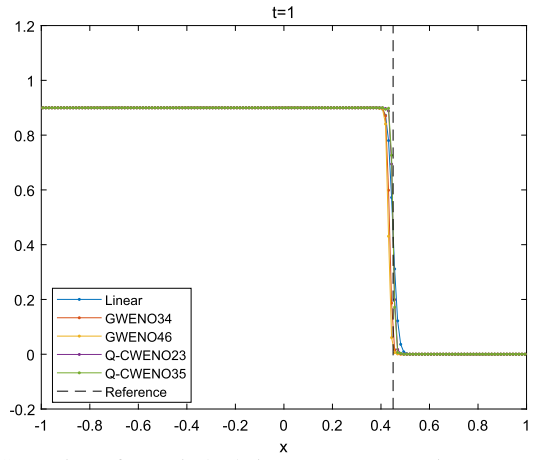

(b) Comparison of numerical solutions w.r.t. reconstruction at $x \in [-1, 1]$

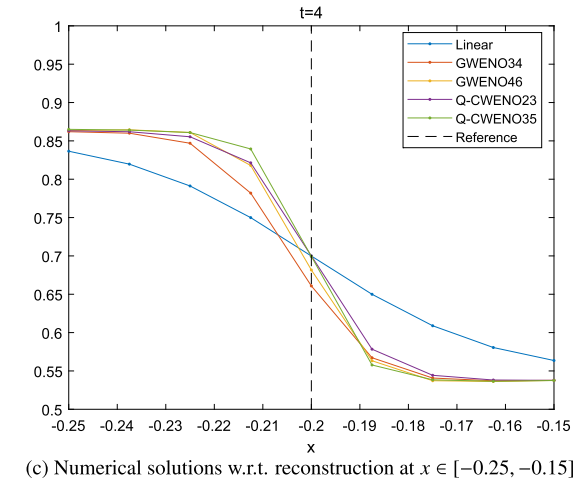

(c) Numerical solutions w.r.t. reconstruction at $x \in [-0.25, -0.15]$

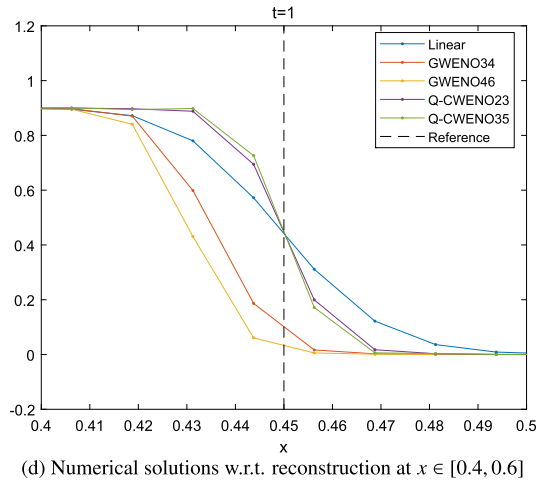

(d) Numerical solutions w.r.t. reconstruction at $x \in [0.4, 0.6]$

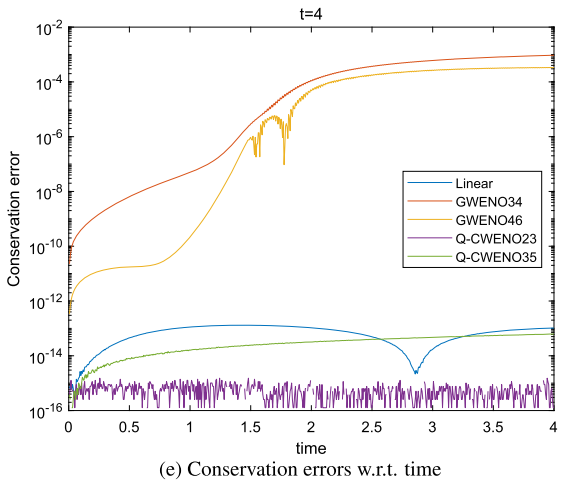

(e) Conservation errors w.r.t. time

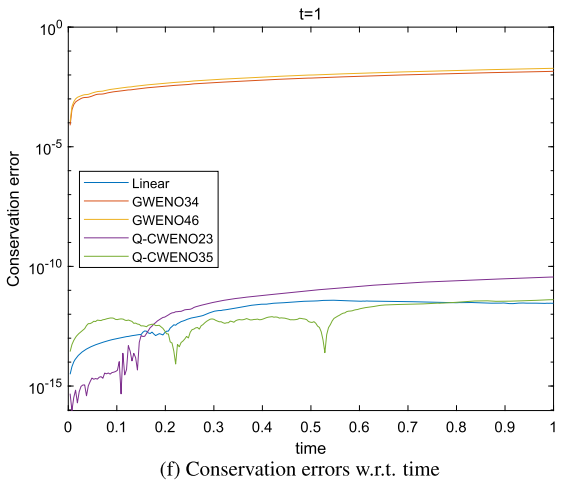

(f) Conservation errors w.r.t. time

Fig. 6. Shock tests for 1D Xin-Jin model. Left: initial data (45) with CFL= 0.5 Right: initial data (46) with CFL= 0.3. The results are obtained by DIRK43 based SL methods for $\kappa = 10^{-8}$ with various reconstructions.

Then, with the initial conditions (46), the following calculation verifies our remark. • Assume CFL= $\frac{\Delta t}{\Delta x} \leq 1$, and $(u^0_{i-2}, u^0_{i-1}, u^0_i, u^0_{i+1}, u^0_{i+2}) = (0.9, 0.9, 0.9, 0.9, 0)$. Then, in the limit $\kappa \to 0$, we have

$$u^1_i = \left(1 - \frac{\Delta t}{\Delta x}\right) u^0_i + \frac{\Delta t}{2\Delta x}(u^0_{i-1} + u^0_{i+1}) + \frac{b\Delta t}{2\Delta x}(u^0_{i-1} - u^0_{i+1}) + \frac{(b^2-1)(\Delta t)^2}{8(\Delta x)^2}(u^0_{i-2} - 2u^0_i + u^0_{i+2})$$

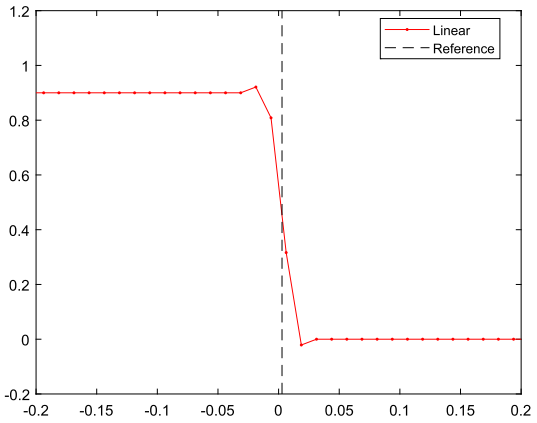

Fig. 7. Shock test associated to Remark 5.1. For $\kappa = 10^{-8}$, DIRK2 based SL scheme is implemented with linear interpolation. Note that oscillation appears at $T^f = \Delta t = 0.00625$.

$$= 0.9\left(1 + \frac{(1-b^2)(\Delta t)^2}{8(\Delta x)^2}\right) > 0.9,$$

for any $\alpha_1 \neq 0, 1$. In [39] the authors show that implicit RK and multistep schemes of order higher than one cannot be a TVD when applied to Burgers equation.

5.2. 1D Broadwell model

Now, we move on to the semi-Lagrangian schemes for 1D Broadwell model (37).

5.2.1. Accuracy test

To check the accuracy of the proposed schemes, we consider well-prepared data [3]:

$$\begin{aligned} &\rho_0(x) = 1 + a_\rho \sin\frac{2\pi}{L}x, \quad u_0(x) = \frac{1}{2} + a_u \sin\frac{2\pi}{L}x, \\ &z_0(x) = z_E(\rho_0(x), u_0(x)) + \kappa z_1(\rho_0(x), u_0(x)) \end{aligned} \tag{47}$$

where $a_\rho = 0.3$, $a_u = 0.1$, $L = 20$, $T^f = 30$, and

$$\begin{aligned} &z_E(\rho_0, m_0) = \frac{1}{2\rho_0}\left(\rho_0^2 + m_0^2\right), \quad z_1(\rho_0, m_0) = -\frac{H(\rho_0, m_0)}{\rho_0}, \\ &H(\rho_0, m_0) = \left(1 - \partial_\rho z_E + (\partial_m z_E)^2\right)\partial_x m_0 + (\partial_\rho z_E \partial_m z_E)\partial_x \rho_0. \end{aligned}$$

The periodic condition is imposed on $[-20, 20]$ upto final time $T^f = 30$. We take different CFL numbers less than 1. The order of convergence is based on the grid points $N_x = 160, 320, 640$. Here the desired accuracy for DIRK2 is between 2 and 3, while for DIRK43, it is between 3 and 5.

In Fig. 8, one can see that the DIRK2 based method attains the desired accuracy for all ranges of κ. On the other hand, in the limit $\kappa \to 0$, the DIRK43 based method shows order reduction, which could be prevented by adopting the BDF3 based method. For small CFL numbers, space errors dominate so the order of accuracy comes from spatial reconstruction, while for large CFL time discretization errors dominate so the order of accuracy comes from time integration.

5.3. Shock tests

We consider a test in [2] with the following initial data:

$$(\rho,\ m,\ z) = \begin{cases} (2, 1, 1) & x < 0.2 \\ (1, 0.13962, 1) & x > 0.2 \end{cases}, \quad x \in [-1, 1]. \tag{48}$$

In Fig. 9, we depict numerical solutions at final time $T^f = 0.5$ using $N_x = 200$. For comparison, we also plot the reference solutions obtained by solving (39) with an Eulerian approach based on finite difference scheme using RK4 and WENO35. To compute the reference solutions, we take a sufficiently small time step $\Delta t = 0.7\Delta x$ with $\Delta x = 0.5 \times 10^{-3}$ for $\kappa = 10^{-q}$,

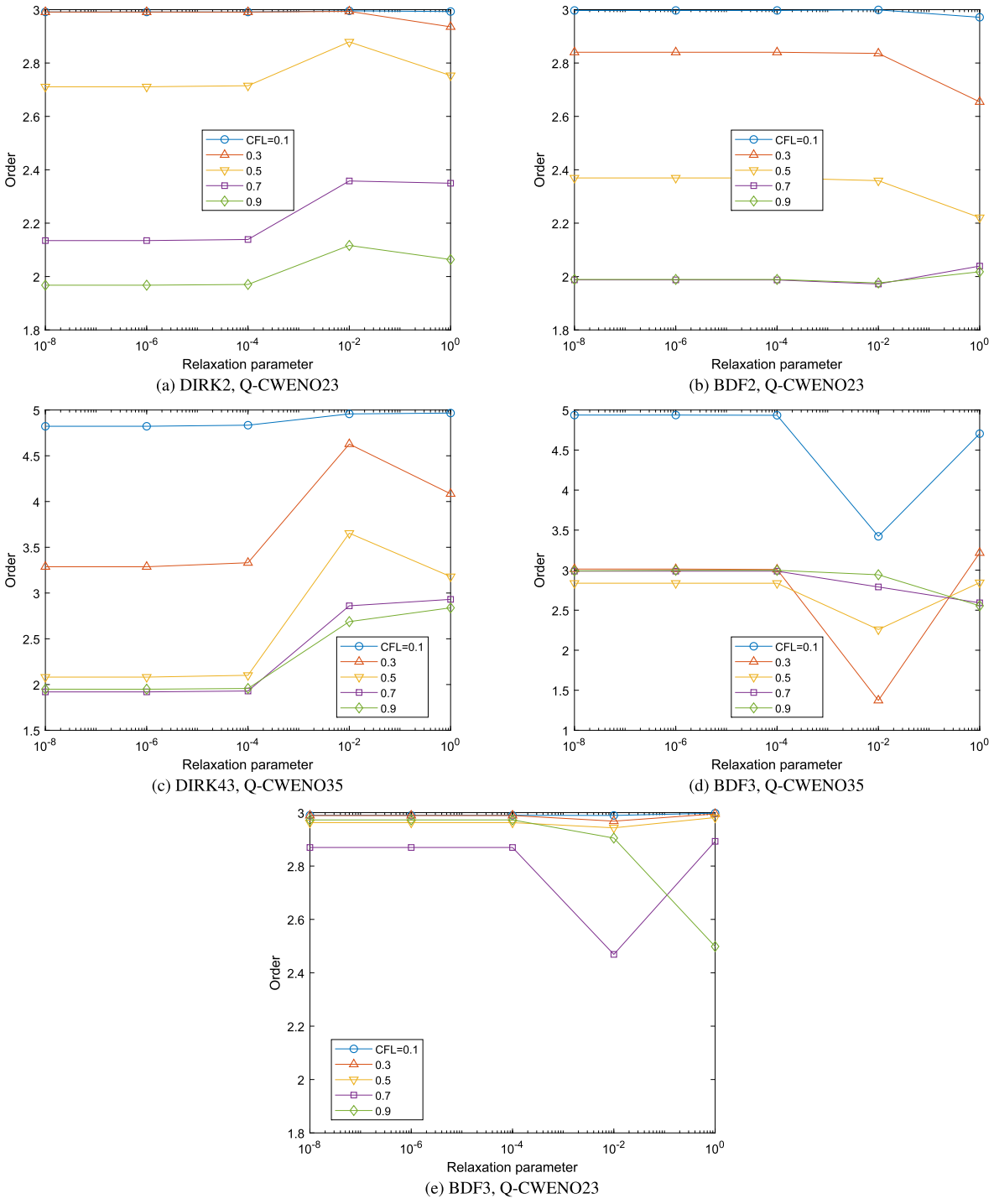

(a) DIRK2, Q-CWENO23

(b) BDF2, Q-CWENO23

(c) DIRK43, Q-CWENO35

(d) BDF3, Q-CWENO35

(e) BDF3, Q-CWENO23

Fig. 8. Accuracy tests for 1D Broadwell model. Initial data is associated to (47). x-axis is for the relaxation parameter κ and y-axis is for order of accuracy based on $N_x = 160, 320, 640$.

$q = 0, 1, 2, 3$. Note that the proposed schemes allow large CFL > 1 with the choice of relatively large relaxation parameters $\kappa = 10^{-q}$, $q = 0, 1, 2$, still showing good agreement to the reference solution. In case of $\kappa = 10^{-3}$, since we observe some oscillations appearing near the discontinuity for CFL > 0.8, we plot solutions for CFL ≤ 0.8. With $\kappa = 10^{-3}$, our solution captures the same shock position of reference solution, and the mismatch around $x = 0$ becomes negligible as we take smaller time steps.

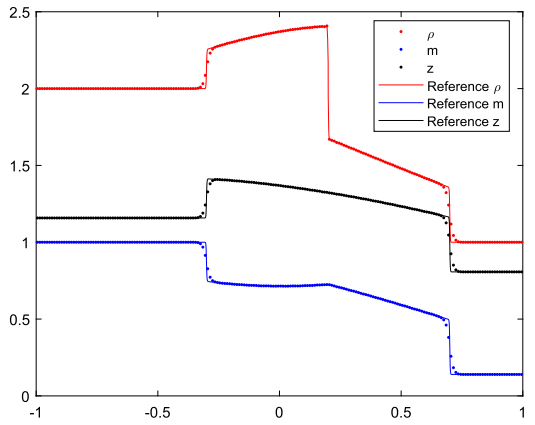

(a) DIRK2, Q-CWENO23, CFL= 2.6, $\kappa = 1$.

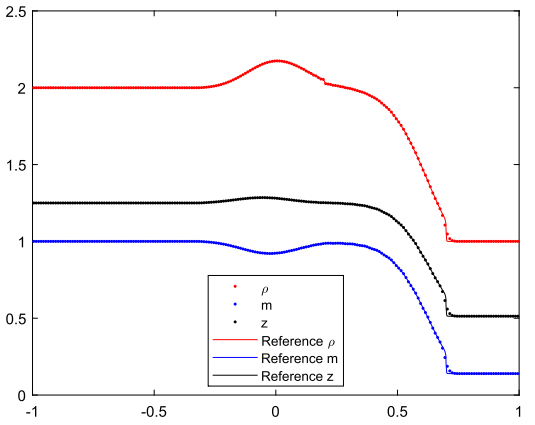

(b) DIRK2, Q-CWENO23, CFL= 2.6, $\kappa = 10^{-1}$.

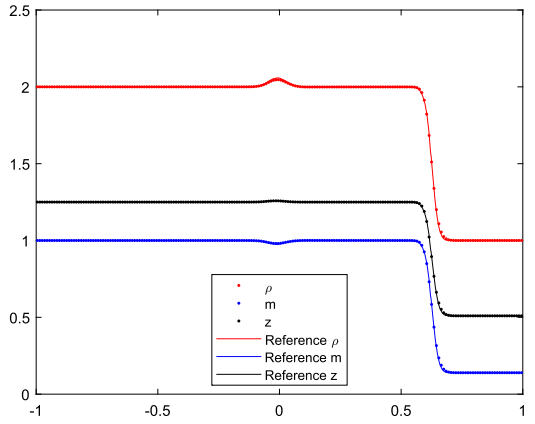

(c) DIRK2, Q-CWENO23, CFL= 1.6, $\kappa = 10^{-2}$.

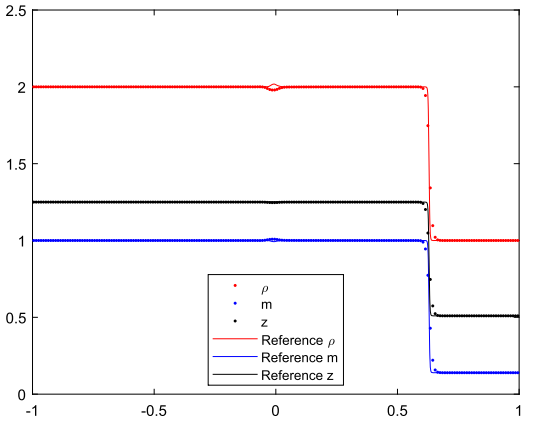

(d) DIRK2, Q-CWENO23, CFL= 0.8, $\kappa = 10^{-3}$.

Fig. 9. Shock tests for 1D Broadwell model. Macroscopic variables ρ (red - top), m (blue - bottom) and z (black - middle). We use the initial data in (48).

5.4. 2D simplified Xin-Jin model

For 2D tests, we here consider the DIRK2 based method.

5.4.1. Accuracy test

Here, we use well-prepared initial data:

$$u_0(x,y) = 0.8\sin^2(\pi x)\sin^2(\pi y), \quad v_0(x,y) = \frac{u_0^2(x,y)}{2} + \kappa\left(u_0^2(x,y) - 1\right)\left(\partial_x u_0(x,y) + \partial_y u_0(x,y)\right). \tag{49}$$

The computation is performed in $(x,y) \in [0,1]^2$ with the periodic boundary condition with $N_x = N_y$. In this problem, the breaking time is $T_b = \dfrac{1}{0.6\pi\sqrt{3}} \approx 0.3063$, we take a final time as $T^f = 0.15$. Since $|u_0| < 1$, the subcharacteristic condition is satisfied. We restrict the ratio to satisfy $\sqrt{2}\dfrac{\Delta t}{\Delta x} = \sqrt{2}\dfrac{\Delta t}{\Delta y} \le 1$. In Fig. 10, we confirm that SL schemes based on DIRK2 and BDF2 attains desired accuracy between 2 and 3 for all ranges of the relaxation parameter κ.

5.4.2. Shock tests

Now, we move on to 2D shock tests for (28).

• **Smooth initial data.** Here, we solve the relaxation system (28) to capture the profile of the shock in Burgers equation. For this, we consider the following initial data:

$$u_0(x,y) = 0.8\sin^2(\pi x)\sin^2(\pi y), \quad v_0(x,y) = \frac{u_0^2(x,y)}{2}, \tag{50}$$

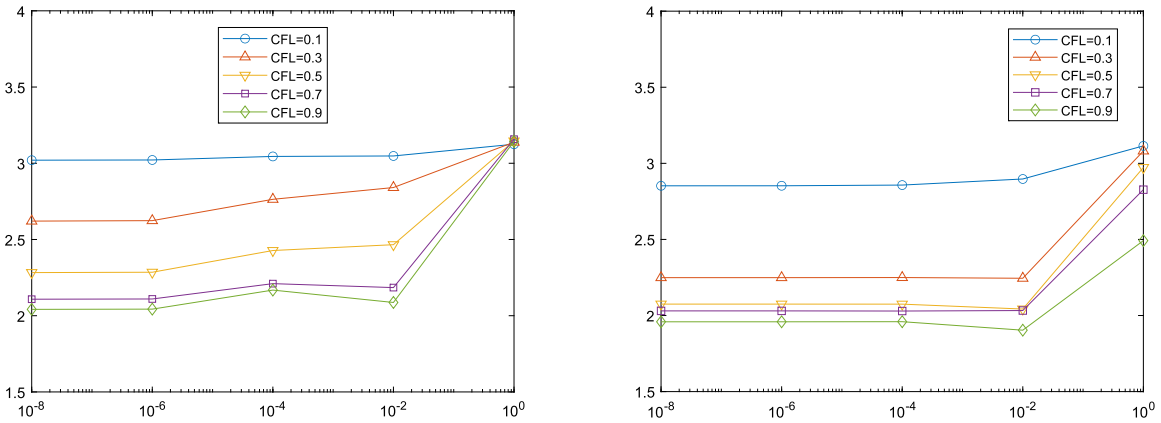

(a) DIRK2 - Q-CWENO23 (b) BDF2 - Q-CWENO23

Fig. 10. Accuracy tests for 2D Xin-Jin model. Initial data is associated to (49). x-axis is for the relaxation parameter κ and y-axis is for order of accuracy based on $N_x^2 = N_y^2 = 160^2, 320^2, 640^2$.

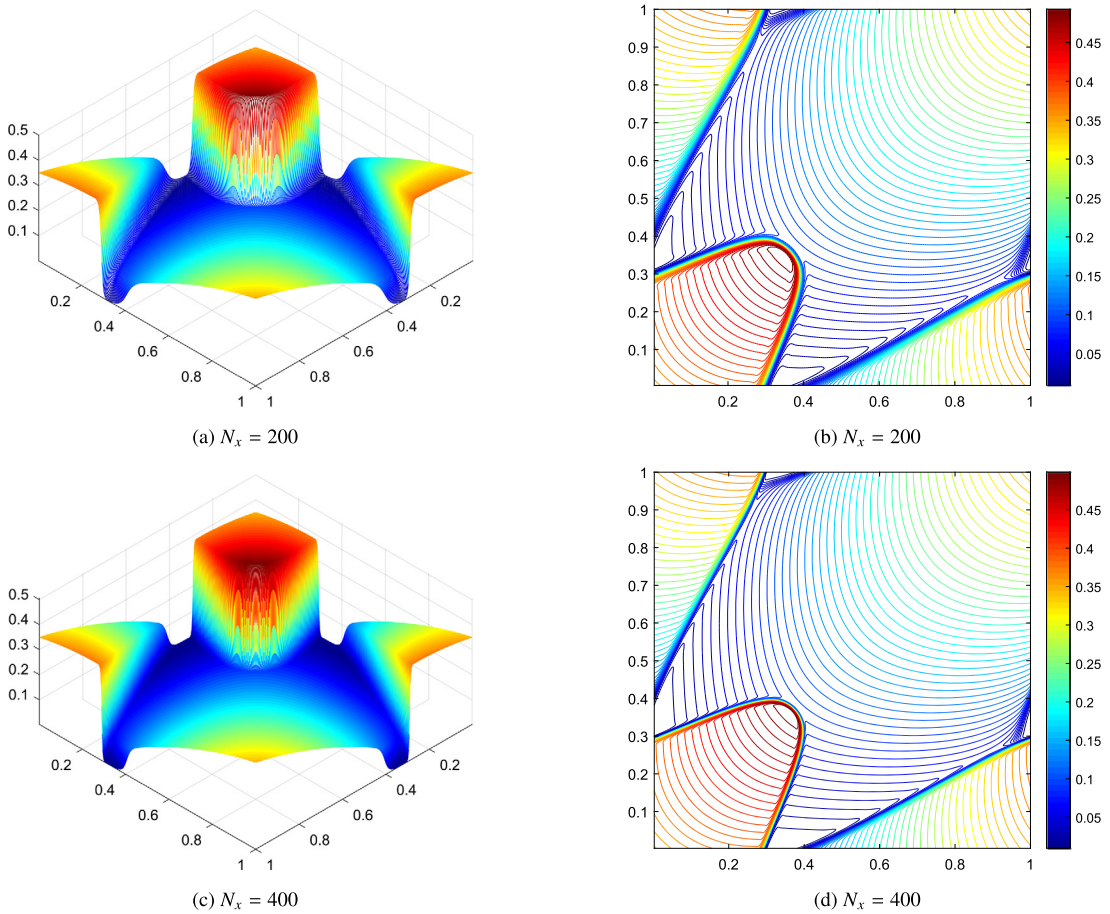

(a) $N_x = 200$ (b) $N_x = 200$

(c) $N_x = 400$ (d) $N_x = 400$

Fig. 11. Shock test for 2D Xin-Jin model. Initial data is associated to (50). Numerical solutions are obtained by DIRK2 based SL scheme for $\kappa = 10^{-4}$. Mesh plot (left) and contour plot (right) of the solution u with $N_x = N_y = 200, 400$.

on the periodic domain $(x, y) \in [0, 1]^2$ with grid points $N_x = N_y = 200, 400$ and mesh ratio $\sqrt{2}\frac{\Delta t}{\Delta x} = \sqrt{2}\frac{\Delta t}{\Delta y} = 0.25$. In Fig. 11, results are reported for $t = 2$. Here, we only present result using 2D SL methods based on DIRK2 and Q-CWENO23.

• **Discontinuous initial data.** This test has been solved by solving a viscous Burgers equation in [40]. Here, we instead solve the relaxation system (28) to capture the correct shock position of Burgers equation. Initial data is given by

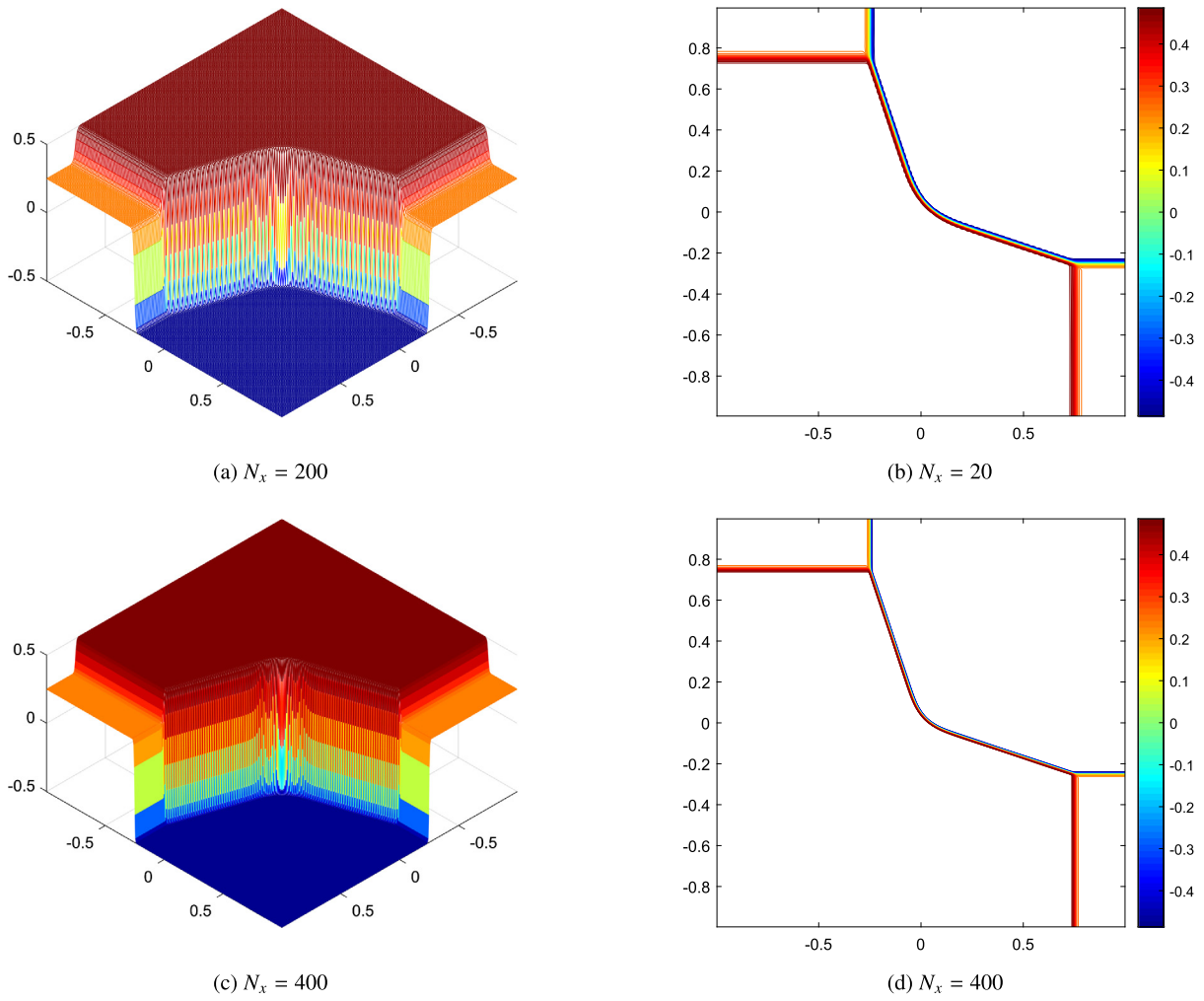

(a) $N_x = 200$ (b) $N_x = 20$

(c) $N_x = 400$ (d) $N_x = 400$

Fig. 12. Shock test for 2D Xin-Jin model. Initial data is associated to (51). Numerical solutions are obtained by DIRK2 based SL scheme for $\kappa = 10^{-4}$. Mesh plot (left) and contour plot (right) of the solution u with $N_x = N_y = 200, 400$.

$$u_0(x) = \begin{cases} -0.5, & x > 0, y > 0 \\ 0.25, & x \le 0, y > 0 \\ 0.25, & x > 0, y \le 0 \\ 0.5, & x \le 0, y \le 0 \end{cases}, \quad v_0(x, y) = \frac{u_0^2(x, y)}{2} \tag{51}$$

with freeflow boundary condition $(x, y) \in [-1, 1].^2$ with grid points $N_x = N_y = 200, 400$ and mesh ratio $\sqrt{2}\frac{\Delta t}{\Delta x} = \sqrt{2}\frac{\Delta t}{\Delta y} = 0.25$. In Fig. 12, we plot the results for $t = 2$. We only present result using 2D SL methods based on DIRK2 and Q-CWENO23.

6. Conclusions

We propose a simple technique to restore conservation in semi-Lagrangian schemes when non-linear reconstructions are adopted to avoid spurious oscillation or to preserve the positivity of the solution. The reconstruction is obtained by taking the sliding average of a basic non-oscillatory (positive-preserving) cell-average to point-wise reconstruction R, thus it inherits the non-oscillatory (positivity-preserving) property of R. A detailed analysis is performed of the proposed reconstruction, proving its accuracy and conservation properties, and its consistency with Lagrange interpolation in the case of linear basic reconstruction. A two-dimensional extension is also considered and analyzed. The technique is then tested on the Xin-Jin relaxation system in one and two space dimensions, and on the 1D Broadwell model. Applications to BGK model and Vlasov-Poisson system will be presented in the second part of the paper.

CRediT authorship contribution statement

Seung Yeon Cho: Formal analysis, Methodology, Software. **Sebastiano Boscarino:** Formal analysis, Methodology, Software. **Giovanni Russo:** Conceptualization, Formal analysis, Methodology. **Seok-Bae Yun:** Formal analysis, Methodology.

Declaration of competing interest

The authors declare that they have no known competing financial interests or personal relationships that could have appeared to influence the work reported in this paper.

Acknowledgements

S. Y. Cho has been supported by ITN-ETN Horizon 2020 Project ModCompShock, Modeling and Computation on Shocks and Interfaces, Project Reference 642768. S.-B. Yun has been supported by Samsung Science and Technology Foundation under Project Number SSTF-BA1801-02. All the authors would like to thank the Italian Ministry of Instruction, University and Research (MIUR) to support this research with funds coming from PRIN Project 2017 (No. 2017KKJP4X entitled "Innovative numerical methods for evolutionary partial differential equations and applications"). S. Boscarino has been supported by the University of Catania ("Piano della Ricerca 2016/2018, Linea di intervento 2"). S. Boscarino and G. Russo are members of the INdAM Research group GNCS.

Appendix A. Proof of Proposition 2.1

Proof. We first write (7) as

$$Q_{i+\theta} = \sum_{\ell=\text{even}}^{k} (\Delta x)^{\ell} \left(\alpha_{\ell}(\theta) R_i^{(\ell)} + \left(\frac{1}{(\ell+1)!} \left(\frac{1}{2} \right)^{\ell} - \alpha_{\ell}(\theta) \right) R_{i+1}^{(\ell)} \right) + \sum_{\ell=\text{odd}}^{k} (\Delta x)^{\ell} \alpha_{\ell}(\theta) \left(R_i^{(\ell)} - R_{i+1}^{(\ell)} \right). \tag{A.1}$$

This, together with the assumption (12), gives

$$\begin{aligned} Q_{i+\theta} &= \sum_{\ell=\text{even}}^{k} (\Delta x)^{\ell} \left(\alpha_{\ell}(\theta) u_i^{(\ell)} + \left(\frac{1}{(\ell+1)!} \left(\frac{1}{2} \right)^{\ell} - \alpha_{\ell}(\theta) \right) u_{i+1}^{(\ell)} \right) + \sum_{\ell=\text{odd}}^{k} (\Delta x)^{\ell} \alpha_{\ell}(\theta) \left(u_i^{(\ell)} - u_{i+1}^{(\ell)} \right) + (\Delta x)^{k+2} \\ &= \sum_{\ell=0}^{k} (\Delta x)^{\ell} \left(\alpha_{\ell}(\theta) u_i^{(\ell)} + \beta_{\ell}(\theta) u_{i+1}^{(\ell)} \right) + (\Delta x)^{k+2}. \end{aligned}$$

Using Taylor's expansion $u_{i+1}^{(\ell)} = u_i^{(\ell)} + u_i^{(\ell+1)} \Delta x + \frac{1}{2} u_i^{(\ell+2)} (\Delta x)^2 + \frac{1}{6} u_i^{(\ell+3)} (\Delta x)^3 + \cdots$, we obtain

$$\begin{aligned} Q_{i+\theta} &= \sum_{\ell=0}^{k} (\Delta x)^{\ell} \left(\alpha_{\ell}(\theta) u_i^{(\ell)} + \beta_{\ell}(\theta) \sum_{m=0}^{k+1-\ell} \frac{u_i^{(\ell+m)}}{m!} (\Delta x)^m \right) + \mathcal{O}\left((\Delta x)^{k+2} \right) \\ &= \sum_{\ell=0}^{k} (\Delta x)^{\ell} \alpha_{\ell}(\theta) u_i^{(\ell)} + \sum_{\ell=0}^{k} \sum_{m=0}^{k-\ell} (\Delta x)^{\ell+m} \beta_{\ell}(\theta) \frac{u_i^{(\ell+m)}}{m!} + \sum_{\ell=0}^{k} (\Delta x)^{k+1} \beta_{\ell}(\theta) \frac{u_i^{(k+1)}}{(k+1-\ell)!} + \mathcal{O}\left((\Delta x)^{k+2} \right) \\ &=: \sum_{\ell=0}^{k} (\Delta x)^{\ell} \lambda_{\ell}(\theta) u_i^{(\ell)} + \sum_{\ell=0}^{k} (\Delta x)^{k+1} \beta_{\ell}(\theta) \frac{u_i^{(k+1)}}{(k+1-\ell)!} + \mathcal{O}\left((\Delta x)^{k+2} \right), \end{aligned}$$

where $\lambda_{\ell}(\theta) = \alpha_{\ell}(\theta) + \sum_{m=0}^{\ell} \beta_m(\theta) \frac{1}{(\ell-m)!}$. Note that

$$\sum_{\ell=0}^{k} \beta_{\ell}(\theta) \frac{1}{(k+1-\ell)!} = \alpha_{k+1}(\theta) + \sum_{m=0}^{k+1} \beta_m(\theta) \frac{1}{(k+1-m)!} = \lambda_{k+1}(\theta).$$

The first equality follows from $\alpha_{k+1}(\theta) + \beta_{k+1}(\theta) = 0$, which holds due to (9) for an even integer k. To sum up,

$$Q_{i+\theta} = \sum_{\ell=0}^{k+1} (\Delta x)^{\ell} \lambda_{\ell}(\theta) u_i^{(\ell)} + \mathcal{O}\left((\Delta x)^{k+2} \right),$$

and this can be written explicitly as follows:

$$
\begin{aligned}
Q_{i+\theta} &= u_i^{(0)} + \theta u_i^{(1)}\Delta x + \left(\frac{\theta^2}{2} + \frac{1}{24}\right) u_i^{(2)}(\Delta x)^2 + \left(\frac{\theta^3}{6} + \frac{\theta}{24}\right) u_i^{(3)}(\Delta x)^3 + \left(\frac{\theta^4}{24} + \frac{\theta^2}{48} + \frac{1}{1920}\right) u_i^{(4)}(\Delta x)^4 \\
&\quad + \left(\frac{\theta^5}{120} + \frac{\theta^3}{144} + \frac{\theta}{1920}\right) u_i^{(5)}(\Delta x)^5 + \left(\frac{\theta^6}{720} + \frac{\theta^4}{576} + \frac{\theta^2}{3840} + \frac{1}{322560}\right) u_i^{(6)}(\Delta x)^6 + \cdots + \mathcal{O}\left((\Delta x)^{k+2}\right) \\
&= \sum_{\ell=0}^{k+1} \frac{\theta^\ell}{\ell!} u_i^{(\ell)}(\Delta x)^\ell + \frac{(\Delta x)^2}{24} \sum_{\ell=0}^{k-1} \frac{\theta^\ell}{\ell!} u_i^{(\ell+2)}(\Delta x)^\ell + \frac{(\Delta x)^4}{1920} \sum_{\ell=0}^{k-3} \frac{\theta^\ell}{\ell!} u_i^{(\ell+4)}(\Delta x)^\ell \\
&\quad + \frac{(\Delta x)^6}{322560} \sum_{\ell=0}^{k-5} \frac{\theta^\ell}{\ell!} u_i^{(\ell+4)}(\Delta x)^\ell + \cdots + \mathcal{O}\left((\Delta x)^{k+2}\right).
\end{aligned}
$$

Consequently, we can derive

$$
\begin{aligned}
Q_{i+\theta} &= u(x_{i+\theta}) + \frac{(\Delta x)^2}{24} u^{(2)}(x_{i+\theta}) + \frac{(\Delta x)^4}{1920} u^{(4)}(x_{i+\theta}) + \cdots + \mathcal{O}\left((\Delta x)^{k+2}\right) \\
&= \sum_{\ell=\text{even}}^{k} (\Delta x)^\ell\, u^{(\ell)}(x_{i+\theta}) \frac{1}{(\ell+1)!}\left(\frac{1}{2}\right)^\ell + \mathcal{O}\left((\Delta x)^{k+2}\right) \\
&= \bar{u}(x_{i+\theta}) + \mathcal{O}\left((\Delta x)^{k+2}\right). \quad \square
\end{aligned}
$$

Appendix B. Proof of Remark 2.2

Consider any polynomial reconstruction $R_i(x), R_{i+1}(x) \in \mathbb{P}^k$ of the form (4) such that

$$
u^{(\ell)}(x_i) - R_i^{(\ell)} = \mathcal{O}\left((\Delta x)^{k+1-\ell}\right), \quad u^{(\ell)}(x_{i+1}) - R_{i+1}^{(\ell)} = \mathcal{O}\left((\Delta x)^{k+1-\ell}\right).
$$

From the assumption that $R_i^{(\ell)}$ is represented by Lipschitz functions F_ℓ of $\{\bar{u}_{i-r}, \cdots, \bar{u}_{i+s}\}$, we can write it as

$$
R_i^{(\ell)} = u^{(\ell)}(x_i) + F_\ell\left(\bar{u}_{i-r}, \cdots, \bar{u}_{i+s}\right) - u^{(\ell)}(x_i),
$$

where $F_\ell\left(\bar{u}_{i-r}, \cdots, \bar{u}_{i+s}\right) - u^{(\ell)}(x_i) = \mathcal{O}\left((\Delta x)^{k+1-\ell}\right)$. Also, in (13), one can see that the function $p_i^{(\ell)} \in \mathbb{P}^{k-\ell}$ is written with a Lipschitz function G_ℓ of $\{\bar{u}_{i-r}, \cdots, \bar{u}_{i+s}\}$ such that

$$
p_i^{(\ell)} = u^{(\ell)}(x_i) + G_\ell\left(\bar{u}_{i-r}, \cdots, \bar{u}_{i+s}\right) - u^{(\ell)}(x_i), \quad G_\ell\left(\bar{u}_{i-r}, \cdots, \bar{u}_{i+s}\right) - u^{(\ell)}(x_i) = \mathcal{O}\left((\Delta x)^{k+1-\ell}\right).
$$

Now, let us define $H_\ell\left(\{\bar{u}_{i-r}, \cdots, \bar{u}_{i+s}\}\right)$ by

$$
H_\ell\left(\bar{u}_{i-r}, \cdots, \bar{u}_{i+s}\right) := G_\ell\left(\bar{u}_{i-r}, \cdots, \bar{u}_{i+s}\right) - F_\ell\left(\bar{u}_{i-r}, \cdots, \bar{u}_{i+s}\right),
$$

then it is Lipschitz continuous w.r.t. $\{\bar{u}_{i-r}, \cdots, \bar{u}_{i+s}\}$ and $H^\ell\left(\bar{u}_{i-r}, \cdots, \bar{u}_{i+s}\right) = \mathcal{O}\left((\Delta x)^{k+1-\ell}\right)$. Consequently,

$$
\begin{aligned}
u^{(\ell)}(x_i) - R_i^{(\ell)} - \left(u^{(\ell)}(x_{i+1}) - R_{i+1}^{(\ell)}\right) &= \left\{u^{(\ell)}(x_i) - p_i^{(\ell)} - \left(u^{(\ell)}(x_{i+1}) - p_{i+1}^{(\ell)}\right)\right\} + \left(p_i^{(\ell)} - R_i^{(\ell)}\right) - \left(p_{i+1}^{(\ell)} - R_{i+1}^{(\ell)}\right) \\
&= \mathcal{O}\left((\Delta x)^{k+2-\ell}\right) + H_\ell\left(\{\bar{u}_{i-r}, \cdots, \bar{u}_{i+s}\}\right) - H_\ell\left(\{\bar{u}_{i+1-r}, \cdots, \bar{u}_{i+1+s}\}\right) \\
&= \mathcal{O}\left((\Delta x)^{k+2-\ell}\right).
\end{aligned}
$$

Appendix C. Reviews on CWENO reconstructions

C.1. CWENO23 reconstruction

Here, we review the CWENO23 scheme described in [13]. We start from a polynomial of degree two $P^i_{OPT}(x)$ which interpolates $\bar{u}_{i-1}, \bar{u}_i, \bar{u}_{i+1}$ in the sense of cell averages:

$$
\frac{1}{\Delta x}\int_{x_{i+l-\frac{1}{2}}}^{x_{i+l+\frac{1}{2}}} P^i_{OPT}(x)\,dx = \bar{u}_{i+l}, \quad l = -1, 0, 1.
$$

Then, this polynomial can be written as $P^i_{OPT}(x) = \tilde{u}_i + \tilde{u}_i'(x - x_i) + \frac{1}{2}\tilde{u}_i''(x - x_i)^2$ with

$$\tilde{u}_i = \bar{u}_i - \frac{1}{24}(\bar{u}_{i+1} - 2\bar{u}_i + \bar{u}_{i-1}), \quad \tilde{u}_i' = \frac{\bar{u}_{i+1} - \bar{u}_{i-1}}{2\Delta x}, \quad \tilde{u}_i'' = \frac{\bar{u}_{i+1} - 2\bar{u}_i + \bar{u}_{i-1}}{(\Delta x)^2},$$

and it gives a third order accurate reconstruction of u in I_i:

$$P^i_{OPT}(x) = u(x) + \mathcal{O}(\Delta x)^3, \quad \forall x \in I_i.$$

In the CWENO23 reconstruction, to avoid oscillations, we use the following convex combination:

$$R_i(x) = \sum_k \omega^i_k P^i_k(x), \quad \sum_k \omega^i_k = 1, \quad \omega^i_k \geq 0, \quad k \in \{L, C, R\} \tag{C.1}$$

where P^i_L and P^i_R are first order polynomials such that

$$\int_{x_{i+l-\frac{1}{2}}}^{x_{i+l+\frac{1}{2}}} P^i_L(x)\,dx = \bar{u}_{i+l}, \quad l = -1, 0, \qquad \int_{x_{i+l-\frac{1}{2}}}^{x_{i+l+\frac{1}{2}}} P^i_R(x)\,dx = \bar{u}_{i+l}, \quad l = 0, 1,$$

which gives

$$P^i_L(x) = \bar{u}_i + \frac{\bar{u}_i - \bar{u}_{i-1}}{\Delta x}(x - x_i), \quad P^i_R(x) = \bar{u}_i + \frac{\bar{u}_{i+1} - \bar{u}_i}{\Delta x}(x - x_i).$$

The second order polynomial $P^i_C(x)$ is obtained from

$$P^i_C(x) := \frac{1}{C_C}\left(P^i_{OPT}(x) - C_L P^i_L(x) - C_R P^i_R(x)\right),$$

with a choice of positive coefficients such that

$$C_L, C_R, C_C \geq 0, \quad C_L = C_R, \quad C_L + C_C + C_R = 1.$$

A common choice is to set $C_L = C_R = 1/4$, $C_C = 1/2$. The non-linear weights ω^i_k in (C.1) are chosen as follows:

$$\omega^i_k = \frac{\alpha^i_k}{\sum_\ell \alpha^i_\ell}, \quad \alpha^i_k = \frac{C_i}{(\epsilon + \beta^i_k)^p}, \quad k, \ell \in \{L, C, R\} \tag{C.2}$$

where the constant ϵ is used to avoid the denominator vanishing and the constant p weights the smoothness indicator. We use $\epsilon = (\Delta x)^2$ or 10^{-6} and $p = 2$ in the numerical tests. An explicit expression of smoothness indicators is the following:

$$\beta^i_L = (\bar{u}_i - \bar{u}_{i-1})^2, \quad \beta^i_R = (\bar{u}_{i+1} - \bar{u}_i)^2,$$
$$\beta^i_C = \frac{13}{3}(\bar{u}_{i+1} - 2\bar{u}_i + \bar{u}_{i-1})^2 + \frac{1}{4}(\bar{u}_{i+1} - \bar{u}_{i-1})^2.$$

We refer to [12] for details on CWENO reconstruction. As a consequence, the reconstruction (C.1) is third order accurate in smooth region and automatically becomes second order accurate in the presence of discontinuity. The final form of the CWENO23 reconstruction $R_i(x)$ is given by

$$R_i(x) = R^{(0)}_i + R^{(1)}_i(x - x_i) + \frac{1}{2}R^{(2)}_i(x - x_i)^2, \tag{C.3}$$

where

$$R^{(0)}_i = \bar{u}_i - \frac{1}{12}\omega^i_C\,(\bar{u}_{i+1} - 2\bar{u}_i + \bar{u}_{i-1})$$
$$R^{(1)}_i = \omega^i_L \frac{\bar{u}_i - \bar{u}_{i-1}}{\Delta x} + \omega^i_R \frac{\bar{u}_{i+1} - \bar{u}_i}{\Delta x} + \omega^i_C \frac{\bar{u}_{i+1} - \bar{u}_{i-1}}{2\Delta x}$$
$$R^{(2)}_i = 2\omega^i_C \frac{\bar{u}_{i+1} - 2\bar{u}_i + \bar{u}_{i-1}}{(\Delta x)^2}.$$

The CWENO23Z reconstruction also takes the form (C.3), but its non-linear weights are calculated as follows:

$$\omega^i_k = \frac{\alpha^i_k}{\sum_\ell \alpha^i_\ell}, \quad \alpha^i_k = C_i\left(1 + \frac{\tau}{\epsilon + \beta^i_k}\right)^p, \quad k, \ell \in \{L, C, R\} \tag{C.4}$$

where $p \geq 1$ and $\tau = \left|\beta^i_R - \beta^i_L\right|$.

Below, we prove that the condition (12) in Proposition 2.1 is satisfied both for CWENO23 and CWENO23Z if a given function u is smooth enough. This shows that the corresponding reconstruction (C.3) becomes a fourth order accurate reconstruction for smooth solutions. We first check if the condition (12) is satisfied by (C.3). For this, we assume that u is smooth enough so that $\omega_C^i = \frac{1}{2} + e_C^i$ for $e_C^i = O((\Delta x)^2)$. We refer to [41] for the assumption. Then, we have

$$\begin{aligned} R_i^{(0)} &= \bar{u}_i - \frac{1}{12}\left(C_C + e_C^i\right)(\bar{u}_{i+1} - 2\bar{u}_i + \bar{u}_{i-1}) \\ &= \bar{u}_i - \frac{1}{12}\left(\frac{1}{2} + \mathcal{O}((\Delta x)^2)\right)\left((\Delta x)^2\bar{u}_i'' + \mathcal{O}((\Delta x)^4)\right) \\ &= \bar{u}_i - \frac{1}{24}\left((\Delta x)^2\bar{u}_i''\right) + \mathcal{O}((\Delta x)^4) \\ &= u_i + \mathcal{O}((\Delta x)^4). \end{aligned} \tag{C.5}$$

Similarly, we write $\omega_L^i = \frac{1}{4} + e_L^i$ and $\omega_R^i = \frac{1}{4} + e_R^i$ with $e_L^i, e_R^i = \mathcal{O}((\Delta x)^2)$. Then,

$$\begin{aligned} R_i^{(1)} &= \omega_L^i \frac{\bar{u}_i - \bar{u}_{i-1}}{\Delta x} + \omega_R^i \frac{\bar{u}_{i+1} - \bar{u}_i}{\Delta x} + \omega_C^i \frac{\bar{u}_{i+1} - \bar{u}_{i-1}}{2\Delta x} \\ &= \left(\frac{1}{4} + e_L^i\right)\left[\bar{u}_i' - \frac{\Delta x}{2}\bar{u}_i'' + \frac{(\Delta x)^2}{6}\bar{u}_i'''\right] + \left(\frac{1}{4} + e_R^i\right)\left[\bar{u}_i' + \frac{\Delta x}{2}\bar{u}_i'' + \frac{(\Delta x)^2}{6}\bar{u}_i'''\right] \\ &\quad + \left(\frac{1}{2} + e_C^i\right)\left[\bar{u}_i' + \frac{1}{6}(\Delta x)^2\bar{u}_i'''\right] + \mathcal{O}((\Delta x)^3) \\ &= \bar{u}_i' + \frac{(\Delta x)^2}{6}\bar{u}_i''' + \mathcal{O}((\Delta x)^3). \end{aligned}$$

In the last equality, we used $\sum_k \omega_k^i = 1$. Hence, we can obtain

$$\begin{aligned} R_i^{(1)} - R_{i+1}^{(1)} &= \bar{u}_i' - \bar{u}_{i+1}' + \frac{(\Delta x)^2}{6}(\bar{u}_i''' - \bar{u}_{i+1}''') + \mathcal{O}((\Delta x)^3) \\ &= \bar{u}_i' - \bar{u}_{i+1}' - \frac{(\Delta x)^2}{24}(\bar{u}_i''' - \bar{u}_{i+1}''') + \mathcal{O}((\Delta x)^3) \\ &= \left(\bar{u}_i' - \frac{(\Delta x)^2}{24}\bar{u}_i'''\right) - \left(\bar{u}_{i+1}' - \frac{(\Delta x)^2}{24}\bar{u}_{i+1}'''\right) + \mathcal{O}((\Delta x)^3) = u_i' - u_{i+1}' + \mathcal{O}((\Delta x)^3). \end{aligned} \tag{C.6}$$

It is straightforward to show that

$$\begin{aligned} R_i^{(2)} = 2\omega_C^i \frac{\bar{u}_{i+1} - 2\bar{u}_i + \bar{u}_{i-1}}{(\Delta x)^2} &= 2\left(\frac{1}{2} + e_C^i\right)\left[\frac{\bar{u}_{i+1} - 2\bar{u}_i + \bar{u}_{i-1}}{(\Delta x)^2}\right] \\ &= \left(1 + \mathcal{O}((\Delta x)^2)\right)\left[\bar{u}_i'' + \frac{(\Delta x)^2}{12}\bar{u}_i^{(4)}\right] = u_i'' + \mathcal{O}((\Delta x))^2. \end{aligned} \tag{C.7}$$

From (C.5), (C.6) and (C.7), we confirm that (C.3) satisfies the condition (15) with $k = 2$.

Consequently, the condition (12) in Proposition 2.1 is satisfied by both CWENO23 and CWENO23Z.

C.2. CWENO35 reconstruction

We can take CWENO35 reconstruction [9] as a basic reconstruction R. Here we represent it as the following explicit form of $R_i(x)$:

$$R_i(x) = \sum_{\ell=0}^{4} \frac{R_i^{(\ell)}}{\ell!}(x - x_i)^{(\ell)}, \tag{C.8}$$

with

$$
\begin{aligned}
R_i^{(0)} &= \omega_C \left(\frac{577}{480}\bar{u}_i - \frac{29}{240}\bar{u}_{i-1} + \frac{19}{960}\bar{u}_{i-2} - \frac{29}{240}\bar{u}_{i+1} + \frac{19}{960}\bar{u}_{i+2} \right) \\
&\quad - \omega_2 \left(\frac{\bar{u}_{i-1} - 26\bar{u}_i + \bar{u}_{i+1}}{24} \right) + \omega_1 \left(\frac{23}{24}\bar{u}_i + \frac{1}{12}\bar{u}_{i-1} - \frac{1}{24}\bar{u}_{i-2} \right) + \omega_3 \left(\frac{23}{24}\bar{u}_i + \frac{1}{12}\bar{u}_{i+1} - \frac{1}{24}\bar{u}_{i+2} \right) \\
R_i^{(1)} &= -\omega_C \frac{8\bar{u}_{i-1} - \bar{u}_{i-2} - 8\bar{u}_{i+1} + \bar{u}_{i+2}}{12\Delta x} + \omega_1 \frac{3\bar{u}_i - 4\bar{u}_{i-1} + \bar{u}_{i-2}}{2\Delta x} - \omega_3 \frac{3\bar{u}_i - 4\bar{u}_{i+1} + \bar{u}_{i+2}}{2\Delta x} - \omega_2 \frac{\bar{u}_{i-1} - \bar{u}_{i+1}}{2\Delta x} \\
R_i^{(2)} &= 2\left(\omega_1 \frac{\bar{u}_i - 2\bar{u}_{i-1} + \bar{u}_{i-2}}{2(\Delta x)^2} + \omega_2 \frac{\bar{u}_{i-1} - 2\bar{u}_i + \bar{u}_{i+1}}{2(\Delta x)^2} + \omega_3 \frac{\bar{u}_i - 2\bar{u}_{i+1} + \bar{u}_{i+2}}{2(\Delta x)^2} \right) \\
&\quad - 2\omega_C \left(\frac{10\bar{u}_i - 6\bar{u}_{i-1} + \bar{u}_{i-2} - 6\bar{u}_{i+1} + \bar{u}_{i+2}}{4(\Delta x)^2} \right) \\
R_i^{(3)} &= 6\omega_C \left(\frac{\bar{u}_{i-1} - \bar{u}_{i+1}}{3(\Delta x)^3} - \frac{\bar{u}_{i-2} - \bar{u}_{i+2}}{6(\Delta x)^3} \right), \quad R_i^{(4)} = 24\omega_C \left(\frac{\bar{u}_{i-2} + 6\bar{u}_i + \bar{u}_{i+2}}{12(\Delta x)^4} - \frac{\bar{u}_{i-1} + \bar{u}_{i+1}}{3(\Delta x)^4} \right),
\end{aligned}
\tag{C.9}
$$

where the non-linear weights ω_k^i are computed as in (C.2). (See also [9].)

The CWENOZ5 reconstruction also can be directly obtained from [11] with the following non-linear weights:

$$
\omega_k^i = \frac{\alpha_k^i}{\sum_\ell \alpha_\ell^i}, \quad \alpha_k^i = C_i \left(1 + \frac{\tau}{\epsilon + \beta_k^i} \right)^t, \quad k, \ell \in \{1, 2, 3, C\}, \tag{C.10}
$$

where $t \geq 1$ and $\tau = |\beta_3^i - \beta_1^i|$.

Appendix D. Proof of Proposition 3.1

Proof. Recall the index set in (25). For each index set, apply corresponding approximations in (24) to (23). Then,

$$
\begin{aligned}
Q_{i+\theta, j+\eta} = \sum_{|\ell|=0}^{k} (\Delta)^\ell \Big(& \alpha_{\ell_1}(\theta)\alpha_{\ell_2}(\eta) u_{i,j}^{(\ell)} + \beta_{\ell_1}(\theta)\alpha_{\ell_2}(\eta) u_{i+1,j}^{(\ell)} \\
& + \alpha_{\ell_1}(\theta)\beta_{\ell_2}(\eta) u_{i,j+1}^{(\ell)} + \beta_{\ell_1}(\theta)\beta_{\ell_2}(\eta) u_{i+1,j+1}^{(\ell)} \Big) + \mathcal{O}(h^{k+2}).
\end{aligned}
\tag{D.1}
$$

Now, we consider Taylor's expansion of $u_{i+1,j}^{(\ell)}, u_{i,j+1}^{(\ell)}, u_{i+1,j+1}^{(\ell)}$:

$$
\begin{aligned}
u_{i+1,j}^{(\ell)} &= \sum_{m_1=0}^{k-|\ell|} \frac{u_{i,j}^{(\ell_1+m_1,\ell_2)}}{m_1!} (\Delta x)^{m_1} + \frac{u_{i,j}^{(\ell_1+k-|\ell|+s,\ell_2)}}{(k-|\ell|+s)!} (\Delta x)^{k-|\ell|+s} \\
u_{i,j+1}^{(\ell)} &= \sum_{m_2=0}^{k-|\ell|} \frac{u_{i,j}^{(\ell_1,\ell_2+m_2)}}{m_2!} (\Delta y)^{m_2} + \frac{u_{i,j}^{(\ell_1,\ell_2+k-|\ell|+s)}}{(k-|\ell|+s)!} (\Delta x)^{k-|\ell|+s} \\
u_{i+1,j+1}^{(\ell)} &= \sum_{|m|=0}^{k-|\ell|} \frac{u_{i,j}^{(\ell+m)}}{m_1! m_2!} (\Delta)^m + \sum_{|m|=k-|\ell|+s} \frac{u_{i,j}^{(\ell+m)}}{m_1! m_2!} (\Delta)^m,
\end{aligned}
$$

where $m = (m_1, m_2)$ is an multi index. Inserting this into (D.1), we obtain

$$
Q_{i+\theta, j+\eta} =: \sum_{|\ell|=0}^{k} (\Delta)^\ell \Lambda_\ell(\theta, \eta) u_{i,j}^{(\ell)} + \Gamma(\theta, \eta) + \mathcal{O}\left(h^{k+2}\right), \tag{D.2}
$$

where $\Lambda_\ell(\theta, \eta)$ and $\Gamma(\theta, \eta)$ are given by

$$
\begin{aligned}
\Lambda_\ell(\theta, \eta) &= \alpha_{\ell_1}(\theta)\alpha_{\ell_2}(\eta) + \alpha_{\ell_2}(\eta) \sum_{m_1=0}^{\ell_1} \beta_{m_1}(\theta) \frac{1}{(\ell_1 - m_1)!} \\
&\quad + \alpha_{\ell_1}(\theta) \sum_{m_2=0}^{\ell_2} \beta_{m_2}(\eta) \frac{1}{(\ell_2 - m_2)!} + \sum_{|m|=0}^{|\ell|} \beta_{m_1}(\theta)\beta_{m_2}(\eta) \frac{1}{(\ell_1 - m_1)!(\ell_2 - m_2)!}
\end{aligned}
$$

$$\Gamma(\theta,\eta)=\sum_{|\ell|=0}^{k}\beta_{\ell_1}(\theta)\alpha_{\ell_2}(\eta)\frac{u_{i,j}^{(\ell_1+k-|\ell|+s,\ell_2)}}{(k-|\ell|+s)!}(\Delta x)^{k-|\ell|+s}(\Delta)^{\ell}$$
$$+\sum_{|\ell|=0}^{k}\alpha_{\ell_1}(\theta)\beta_{\ell_2}(\eta)\frac{u_{i,j}^{(\ell_1,\ell_2+k-|\ell|+s)}}{(k-|\ell|+s)!}(\Delta y)^{k-|\ell|+s}(\Delta)^{\ell}+\sum_{|\ell|=0}^{k}\beta_{\ell_1}(\theta)\beta_{\ell_2}(\eta)\sum_{|m|=k-|\ell|+s}\frac{u_{i,j}^{(\ell+m)}}{m_1!m_2!}(\Delta)^{m+\ell}.$$

Now, we add 0 to $\Gamma(\theta,\eta)$ using the following identity:

$$\begin{aligned}0&=\sum_{|\ell|=k+1}\left(\alpha_{\ell_1}(\theta)+\beta_{\ell_1}(\theta)\right)\left(\alpha_{\ell_2}(\eta)+\beta_{\ell_2}(\eta)\right)u_{i,j}^{(\ell)}(\Delta)^{\ell}\\&=\sum_{|\ell|=k+1}\alpha_{\ell_1}(\theta)\alpha_{\ell_2}(\eta)u_{i,j}^{(\ell)}(\Delta)^{\ell}+\sum_{|\ell|=k+1}\beta_{\ell_1}(\theta)\alpha_{\ell_2}(\eta)u_{i,j}^{(\ell)}(\Delta)^{\ell}\\&\quad+\sum_{|\ell|=k+1}\alpha_{\ell_1}(\theta)\beta_{\ell_2}(\eta)u_{i,j}^{(\ell)}(\Delta)^{\ell}+\sum_{|\ell|=k+1}\beta_{\ell_1}(\theta)\beta_{\ell_2}(\eta)u_{i,j}^{(\ell)}(\Delta)^{\ell},\end{aligned}\tag{D.3}$$

then

$$\Gamma(\theta,\eta)+0=\sum_{|\ell|=k+1}\alpha_{\ell_1}(\theta)\alpha_{\ell_2}(\eta)u_{i,j}^{(\ell)}(\Delta)^{\ell}+\sum_{|\ell|=0}^{k+1}\beta_{\ell_1}(\theta)\alpha_{\ell_2}(\eta)\frac{u_{i,j}^{(\ell_1+k-|\ell|+s,\ell_2)}}{(k-|\ell|+s)!}(\Delta x)^{k-|\ell|+s}(\Delta)^{\ell}$$
$$+\sum_{|\ell|=0}^{k+1}\alpha_{\ell_1}(\theta)\beta_{\ell_2}(\eta)\frac{u_{i,j}^{(\ell_1,\ell_2+k-|\ell|+s)}}{(k-|\ell|+s)!}(\Delta y)^{k-|\ell|+s}(\Delta)^{\ell}+\sum_{|\ell|=0}^{k+1}\beta_{\ell_1}(\theta)\beta_{\ell_2}(\eta)\sum_{|m|=k-|\ell|+s}\frac{u_{i,j}^{(\ell+m)}}{m_1!m_2!}(\Delta)^{m+\ell}.$$

This reduces to

$$\Gamma(\theta,\eta)=\sum_{|\ell|=k+1}(\Delta)^{\ell}\Lambda_{\ell}(\theta,\eta)u_{i,j}^{(\ell)}.$$

Based on this formula, we rearrange all terms in (D.2) as follows:

$$\begin{aligned}Q_{i+\theta,j+\eta}&=u_{i,j}+\theta\Delta x u_{i,j}'+\eta\Delta y u_{i,j}^{\backprime}+\left(\frac{\theta^2}{2}+\frac{1}{24}\right)(\Delta x)^2u_{i,j}''+\left(\frac{\eta^2}{2}+\frac{1}{24}\right)(\Delta y)^2u_{i,j}^{\backprime\backprime}+\eta\theta\Delta x\Delta y u_{i,j}^{\prime\backprime}\\&\quad+\left(\frac{\theta^3}{6}+\frac{\theta}{24}\right)(\Delta x)^3u_{i,j}'''+\left(\frac{\eta\theta^2}{2}+\frac{\eta}{24}\right)(\Delta x)^2\Delta y u_{i,j}^{\prime\prime\backprime}\\&\quad+\left(\frac{\theta\eta^2}{2}+\frac{\theta}{24}\right)\Delta x(\Delta y)^2u_{i,j}^{\prime\backprime\backprime}+\left(\frac{\eta^3}{6}+\frac{\eta}{24}\right)(\Delta y)^3u_{i,j}^{\backprime\backprime\backprime}\\&\quad+\cdots+\mathcal{O}(h^{k+2})\\&=u_{i+\theta,j+\eta}+\frac{(\Delta x)^2}{24}u_{i+\theta,j+\eta}''+\frac{(\Delta y)^2}{24}u_{i+\theta,j+\eta}^{\backprime\backprime}+\cdots+\mathcal{O}(h^{k+2})\\&=\bar{u}_{i+\theta,j+\eta}+\mathcal{O}(h^{k+2}),\end{aligned}$$

which completes the proof. □

Appendix E. Semi-Lagrangian schemes for hyperbolic system with BDF methods

The BDF methods [32] for an ordinary system $y'(t)=f(y)$ can be represented by

$$y^{n+1}=\sum_{k=1}^{s}a_k y^{n+1-s}+\beta_s f^{n+1},$$

where α_k and β_s are coefficients corresponding to s-order BDF methods. Here, we consider two cases $s=2,3$:

$$\text{BDF2:}\quad y^{n+1}=\frac{4}{3}y^n-\frac{1}{3}y^{n-1}+\frac{2}{3}f^{n+1}$$
$$\text{BDF3:}\quad y^{n+1}=\frac{18}{11}y^n-\frac{9}{11}y^{n-1}+\frac{2}{11}y^{n-1}+\frac{6}{11}f^{n+1}.$$

E.1. BDF methods for Xin-Jin model

Applying BDF method based SL methods to (32), we obtain:

$$\begin{aligned} f_i^{n+1} &= \sum_{k=1}^{s} \alpha_k \tilde{f}^{n,k} + \beta_s \frac{\Delta t}{\kappa} K_{i,1}^{n+1} \\ g_i^{n+1} &= \sum_{k=1}^{s} \alpha_k \tilde{g}^{n,k} + \beta_s \frac{\Delta t}{\kappa} K_{i,2}^{n+1}. \end{aligned} \tag{E.1}$$

Here we use the following notation:

- For $k = 1, \dots, s$, the $(n+1-k)$th stage values of f, g along the backward-characteristics which come from x_i with characteristic speed $-1, 1$ at time t^{n+1}:

$$\tilde{f}_i^{n,k} \approx f(x_i + k\Delta t, t^{n+1-k}), \quad \tilde{g}_i^{n,k} \approx g(x_i - k\Delta t, t^{n+1-k}).$$

- Fluxes at time t^{n+1}:

$$K_{i,1}^{n+1} \approx F(u_i^{n+1}) - v_i^{n+1}, \quad K_{i,2}^{n+1} \approx -K_{i,1}^{n+1}.$$

The procedure for BDF based methods are simpler than DIRK based methods. At first, for $k = 1, 2, \dots, s$ we interpolate $\tilde{f}_i^{n,k}$ and $\tilde{g}_i^{n,k}$ on $x_i + k\Delta t$ and $x_i - k\Delta t$ from $\{f_i^{n+1-k}\}$ and $\{g_i^{n+1-k}\}$, respectively. Then, by summing and subtracting two equations in (E.1), we compute:

$$\begin{aligned} u_i^{n+1} &= \frac{\sum_{k=1}^{s} \alpha_k \left(\tilde{g}_i^{n,k} + \tilde{f}_i^{n,k} \right)}{2} \\ v_i^{n+1} &= \frac{\kappa \sum_{k=1}^{s} \alpha_k \left(\tilde{g}_i^{n,k} - \tilde{f}_i^{n,k} \right)/2 + \beta_k \Delta t F\left(u_i^{n+1} \right)}{\kappa + \beta_s \Delta t}. \end{aligned}$$

Then, we recover

$$f_i^{n+1} = u_i^{n+1} - v_i^{n+1}, \quad g_i^{n+1} = u_i^{n+1} + v_i^{n+1}.$$

E.2. BDF methods for Broadwell model

Now, we extend this to high order s-order BDF methods. The solutions are obtained by

$$\begin{aligned} f_i^{n+1} &= F_i^n + \frac{\beta_s \Delta t}{\kappa} Q_i^{n+1}, \quad F_i^n := \sum_{\ell=1}^{s} \alpha_k f_i^{n,k}, \\ g_i^{n+1} &= G_i^n + \frac{\beta_s \Delta t}{\kappa} Q_i^{n+1}, \qquad G_i^n := \sum_{\ell=1}^{s} \alpha_k g_i^{n,k}, \\ h_i^{n+1} &= H_i^n - \frac{\beta_s \Delta t}{\kappa} Q_i^{n+1}, \quad H_i^n := \sum_{\ell=1}^{s} \alpha_k h_i^{n+1-k}, \end{aligned} \tag{E.2}$$

where

$$Q_i^{n+1} = (h_i^{n+1})^2 - f_i^{n+1} g_i^{n+1}, \quad f_i^{n,k} \approx f(x_i - k\Delta t, t^{n+1-k}), \quad g_i^{n,k} \approx g(x_i + k\Delta t, t^{n+1-k}).$$

Then, we can update solutions by solving (E.2) as follows:

$$\begin{aligned} h_i^{n+1} &= \frac{\beta_s \Delta t (H_i^n + F_i^n)(H_i^n + G_i^n) + \kappa H_i^n}{\beta_s \Delta t \left(G_i^n + 2H_i^n + F_i^n \right) + \kappa}, \\ f_i^{n+1} &= H_i^n + F_i^n - h_i^{n+1}, \qquad g_i^{n+1} = H_i^n + G_i^n - h_i^{n+1}. \end{aligned}$$

References

[1] C. Cercignani, The Boltzmann Equation and Its Applications, Springer, New York, 1988.
[2] R.E. Caflisch, S. Jin, G. Russo, Uniformly accurate schemes for hyperbolic systems with relaxation, SIAM J. Numer. Anal. 34 (1997) 246–281.
[3] L. Pareschi, G. Russo, Implicit–explicit Runge–Kutta schemes and applications to hyperbolic systems with relaxation, J. Sci. Comput. 25 (2005) 129–155.
[4] S. Jin, Asymptotic preserving (AP) schemes for multiscale kinetic and hyperbolic equations: a review, in: Lecture Notes for Summer School on "Methods and Models of Kinetic Theory" (M&MKT), Porto Ercole, Grosseto, Italy, in: Riv. Math. Univ. Parma, vol. 3, 2010, pp. 177–216.
[5] C.W. Shu, Essentially non-oscillatory and weighted essentially non-oscillatory schemes for hyperbolic conservation laws, in: Advanced Numerical Approximation of Nonlinear Hyperbolic Equations, Springer, 1998, pp. 325–432.
[6] E. Carlini, R. Ferretti, G. Russo, A weighted essentially nonoscillatory, large time-step scheme for Hamilton–Jacobi equations, SIAM J. Sci. Comput. 27 (2005) 1071–1091.
[7] M. Castro, B. Costa, W.S. Don, High order weighted essentially non-oscillatory WENO-Z schemes for hyperbolic conservation laws, J. Comput. Phys. 230 (2011) 1766–1792.
[8] Y.Y. Liu, C.W. Shu, M.P. Zhang, On the positivity of linear weights in WENO approximations, Acta Math. Appl. Sin. 25 (2009) 503–538.
[9] G. Capdeville, A central WENO scheme for solving hyperbolic conservation laws on non-uniform meshes, J. Comput. Phys. 227 (2008) 2977–3014.
[10] I. Cravero, G. Puppo, M. Semplice, G. Visconti, CWENO: uniformly accurate reconstructions for balance laws, Math. Comput. 87 (2017) 1689–1719.
[11] I. Cravero, G. Puppo, M. Semplice, G. Visconti, Cool WENO schemes, Comput. Fluids 169 (2018) 71–86.
[12] D. Levy, G. Puppo, G. Russo, Central WENO schemes for hyperbolic systems of conservation laws, ESAIM: Math. Model. Numer. Anal. 33 (1999) 547–571.
[13] D. Levy, G. Puppo, G. Russo, Compact central WENO schemes for multidimensional conservation laws, SIAM J. Sci. Comput. 22 (2000) 656–672.
[14] D. Levy, G. Puppo, G. Russo, A fourth order central WENO scheme for multidimensional hyperbolic systems of conservation laws, SIAM J. Sci. Comput. 24 (2002) 480–506.
[15] M. Dumbser, W. Boscheri, M. Semplice, G. Russo, Central weighted ENO schemes for hyperbolic conservation laws on fixed and moving unstructured meshes, SIAM J. Sci. Comput. 39 (2017) A2564–A2591.
[16] J.A. Carrillo, F. Vecil, Nonoscillatory interpolation methods applied to Vlasov-based models, SIAM J. Sci. Comput. 29 (2007) 1179–1206.
[17] M. Campos-Pinto, F. Charles, B. Després, Algorithms for positive polynomial approximation, SIAM J. Numer. Anal. 57 (2019) 148–172.
[18] J.W. Schmidt, W. Hess, Positivity of cubic polynomials on intervals and positive spline interpolation, BIT Numer. Math. 28 (1988) 340–352.
[19] S. Boscarino, S.-Y. Cho, G. Russo, S.-B. Yun, High order conservative semi-Lagrangian scheme for the BGK model of the Boltzmann equation, Commun. Comput. Phys. 29 (2021) 1–56.
[20] F. Filbet, E. Sonnendrücker, P. Bertrand, Conservative numerical schemes for the Vlasov equation, J. Comput. Phys. 172 (2001) 166–187.
[21] N. Crouseilles, M. Mehrenberger, E. Sonnendrücker, Conservative semi-Lagrangian schemes for Vlasov equations, J. Comput. Phys. 229 (2010) 1927–1953.
[22] J.M. Qiu, C.W. Shu, Conservative semi-Lagrangian finite difference WENO formulations with applications to the Vlasov equation, Commun. Comput. Phys. 10 (2011) 979–1000.
[23] J.M. Qiu, C.W. Shu, Conservative high order semi-Lagrangian finite difference WENO methods for advection in incompressible flow, J. Sci. Comput. 230 (2011) 863–889.
[24] G. Russo, J. Qiu, X. Tao, Conservative multi-dimensional semi-Lagrangian finite difference scheme: stability and applications to the kinetic and fluid simulations, J. Sci. Comput. (2018) 1–30.
[25] R. Ferretti, Stability of some generalized Godunov schemes with linear high-order reconstructions, J. Sci. Comput. 57 (2013) 213–228.
[26] X. Zhang, C.-W. Shu, On maximum-principle-satisfying high order schemes for scalar conservation laws, J. Comput. Phys. 229 (2010) 3091–3120.
[27] X. Zhang, C.-W. Shu, Maximum-principle-satisfying and positivity-preserving high-order schemes for conservation laws: survey and new developments, Proc. R. Soc. A, Math. Phys. Eng. Sci. 467 (2011) 2752–2776.
[28] J. Friedrich, O. Kolb, Maximum principle satisfying CWENO schemes for nonlocal conservation laws, SIAM J. Sci. Comput. 41 (2019) A973–A988.
[29] F. Filbet, E. Sonnendrücker, Comparison of Eulerian Vlasov solvers, Comput. Phys. Commun. 150 (2001) 247–266.
[30] S. Jin, C.D. Levermore, Numerical schemes for hyperbolic conservation laws with stiff relaxation terms, J. Comput. Phys. 126 (1996) 449–467.
[31] J.E. Broadwell, Shock structure in a simple discrete velocity gas, Phys. Fluids 7 (1964) 1243–1247.
[32] E. Hairer, G. Warner, Solving Ordinary Differential Equations II: Stiff and Differential-Algebraic Problems, Springer, Berlin, 1996.
[33] E. Hairer, G. Warner, S.P. Nórsett, Solving Ordinary Differential Equations I: Nonstiff Problem, Springer, Berlin, 1996.
[34] C. Kennedy, M.H. Carpenter, Additive Runge–Kutta schemes for convection–diffusion–reaction equations, Appl. Numer. Math. 44 (2003) 139–181.
[35] G.Q. Chen, C.D. Levermore, T.P. Liu, Hyperbolic conservation laws with stiff relaxation terms and entropy, Commun. Pure Appl. Math. 47 (1994) 787–830.
[36] S. Jin, Z. Xin, The relaxation schemes for systems of conservation laws in arbitrary space dimensions, Commun. Pure Appl. Math. 48 (1995) 235–276.
[37] S. Boscarino, G. Russo, On a class of uniformly accurate IMEX Runge–Kutta schemes and applications to hyperbolic systems with relaxation, SIAM J. Sci. Comput. 31 (2009) 1926–1945.
[38] G.B. Whitham, Linear and Nonlinear Waves, John Wiley and Sons, New York, 1974.
[39] S. Gottlieb, C.W. Shu, E. Tadmor, Strong stability-preserving high-order time discretization methods, SIAM Rev. 43 (2001) 89–112.
[40] M. Dehghan, M. Abbaszadeh, The space-splitting idea combined with local radial basis function meshless approach to simulate conservation laws equations, Alex. Eng. J. 57 (2018) 1137–1156.
[41] O. Kolb, On the full and global accuracy of a compact third order WENO scheme, SIAM J. Numer. Anal. 52 (2014) 2335–2355.